METAL–SEMICONDUCTOR TRANSITIONS IN NANOSCALE VANADIUM DIOXIDE—THIN FILMS, SUBWAVELENGTH HOLES, AND NANOPARTICLES

By

Eugenii U. Donev

Dissertation

Submitted to the Faculty of the

Graduate School of Vanderbilt University

in partial fulfillment of the requirements

for the degree of

DOCTOR OF PHILOSOPHY

in

Physics

December 2008

Nashville, Tennessee

Approved:

Leonard C. Feldman

Richard F. Haglund, Jr.

Deyu Li

James H. Dickerson

Sharon M. Weiss

CHAPTER IV

USING THE METAL-SEMICONDUCTOR TRANSITION OF VO_2 TO CONTROL OPTICAL TRANSMISSION THROUGH SUBWAVELENGTH HOLE ARRAYS

Abstract

This chapter describes a novel configuration in which the extraordinary optical transmission effect through subwavelength hole arrays in noble-metal films can be switched by the metal-semiconductor transition in an underlying thin film of vanadium dioxide. In these experiments, the transition is brought about by thermal heating of the double-layer film. The surprising reverse hysteretic behavior of the transmission through the subwavelength holes in the vanadium-dioxide layer suggest that this modulation is accomplished by a dielectric-matching condition rather than plasmon coupling through the double-layer film. The results of this switching, including the wavelength dependence, are qualitatively reproduced by a transfer matrix model. The prospects for effecting a similar modulation on a much faster time scale by using ultrafast laser pulses to trigger the metal-semiconductor transition are also discussed.

4.1 Introduction

4.1.1 Motivation

Ever since its initial description in a much-cited letter by Ebbesen *et al.*,[6] the phenomenon of *extraordinary optical transmission* (EOT) has generated intense interest regarding both the fundamental physics of the transmission mechanism as well as potential applications. In brief, the EOT effect refers to the observations that light transmission through periodic arrays of subwavelength holes in opaque thin films can be much larger

than the combined transmission for isolated holes predicted by standard diffraction theory,[142,143] and that the spectral profile of the transmission follows a sequence of dips and peaks peculiar to the materials involved and the detailed geometry of the hole array. This effect has been described predominantly in terms of light waves coupled to collective oscillations of the free electrons, the so-called propagating surface plasmons or surface-plasmon polaritons (SPPs), although recent theoretical developments have identified another surface-wave contribution to the EOT effect in addition to SPPs.[144]

Numerous applications of EOT have been proposed and, in some cases, realized in practice. Specific applications of subwavelength holes[8] include SPP-activated lithographic masks, bright point sources, SPP couplers/decouplers, near-field optical storage heads, molecular sensors, and so on. Recent work[145] has shown that the electroluminescence efficiency of an organic light-emitting diode (OLED) can be significantly enhanced by use of a perforated anode, which allows for light emission from both the back and the front of the device. Control of EOT through a hole array could make it possible, for example, to modulate selectively in wavelength and time the light emitted by an OLED or other sources, or the propagation of light in a waveguide, in effect serving as a subwavelength optical switch. However, there are few reports on methods for post-fabrication modulation of the EOT at visible and near-infrared wavelengths, and both involve varying the refractive index of the input side dielectric. In one case, the authors[146] used different index-matching liquids to vary the degree of asymmetry between the dielectric layer above a perforated gold film and the quartz substrate. The other scheme[7] entailed sandwiching a layer of liquid crystal between a transparent indium-tin-oxide electrode and a perforated chromium film on quartz, then varying the applied electric field. Ultrafast switching of THz signals through metallic subwavelength hole arrays has also been reported.[147]

Here we recount another recently demonstrated method to control the amount of light transmitted through perforated double-layer thin films on transparent substrates, as described in our publications in References [124,125,148]. The structures consist of an optically

opaque silver (Ag) or gold (Au) film on top of a vanadium dioxide (VO_2) film deposited on a glass substrate, with a periodic array of subwavelength holes penetrating the double layer. The intensity of transmitted light is controlled by means of a reversible metal-semiconductor phase transition, thermally induced in the VO_2 layer, which undergoes drastic changes in its electrical and optical properties.

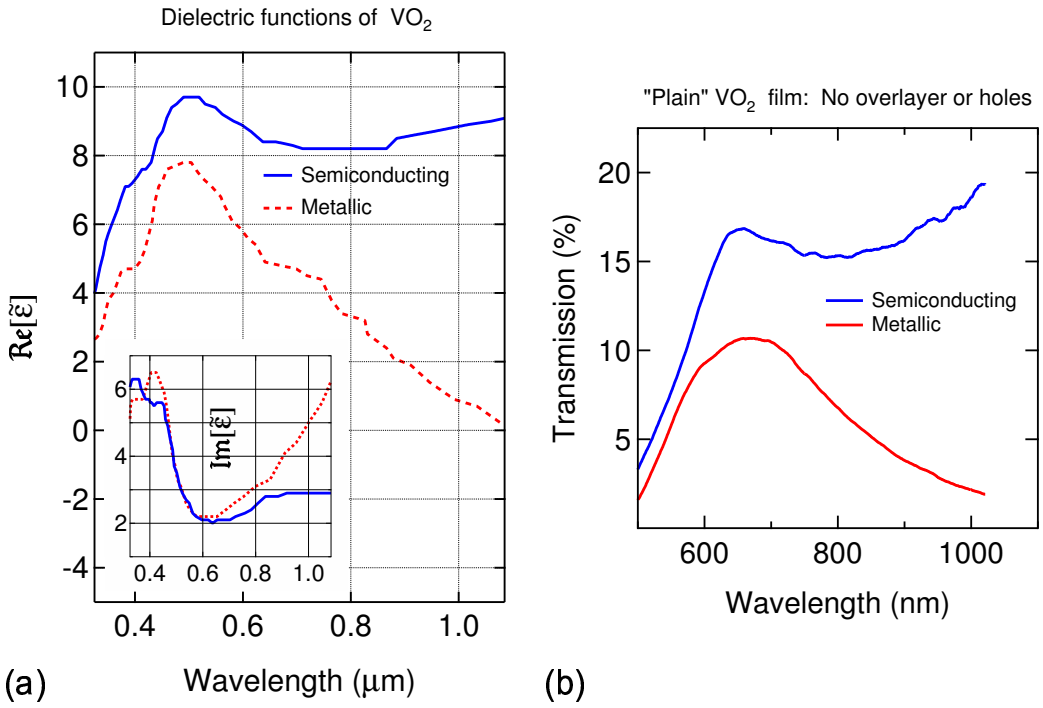

Figure 4.1: **(a)** Real and imaginary parts of relative permittivity of VO_2 (data extracted from Reference [57]). **(a)** Experimental normal-incidence transmission spectra of non-perforated 200-nm thick VO_2 film on glass.

Briefly, the phase transition of VO_2 is a first-order transformation that occurs at a critical temperature $T_c \approx 67^oC$, from a high-temperature metallic phase to a low-temperature semiconducting phase.[21] The precise mechanism of the phase transition has long been a topic of controversy,[25–29] and the cause-and-effect debate over the relative roles of lattice distortion and electron-electron correlations in triggering the VO_2 phase transition has

lately received renewed theoretical[30] and experimental[1–3,31,32] attention. The presence of thermal hysteresis, attributed to variations in the phase-equilibrium temperatures for film grains of different sizes,[81] allows for potential applications in memory devices and optical data storage, while the speed of the transition—about 80 fs according to Cavalleri *et al.*[31]—makes VO_2 a candidate for applications in ultrafast optical switching.[54] Above T_c, VO_2 exhibits metallic character with relatively high opacity in the infrared (IR) wavelength range. Below T_c, the dimerization and tilting of the V–V pairs result in the opening of a narrow band-gap;[22] in this semiconducting phase, films thicker than 100 nm are markedly more transparent in the (near-)IR range with respect to the metallic phase (Figure 4.1). Surprisingly, however, our metal-VO_2 structures exhibit larger near-IR transmission with the VO_2 layer in the metallic state as compared to transmission in the semiconducting state—quite the opposite of the conventional behavior of a "plain" (*i.e.*, no metal overlayer or holes) VO_2 film of the same thickness. This *reverse switching* can be understood in terms of a simple model that takes into account the losses due to *leaky evanescent waves* in the plane of the VO_2 layer and *diffuse scattering* from the holes at the entrance and exit apertures. Numerical simulations based on the transfer matrix formalism for photonic crystals[149] provide qualitative support for the experimental findings.

4.1.2 Extraordinary optical transmission (EOT) and the surface-plasmon polariton (SPP)

A short account of the EOT phenomenon follows in this section. One of Ebbesen *et al.*'s initial EOT results[6] is reproduced in Figure 4.2. It shows a typical zero-order (*i.e.*, the incident and detected light beams being collinear) transmission spectrum for a Ag film perforated by a square array of cylindrical subwavelength holes. Ebbesen and his colleagues termed the transmission "extraordinary" partly because of the very large enhancements at the observed IR peaks over the theoretical prediction for the transmission efficiency of a very small circular aperture in a thin screen of a perfect conductor. The theory, first developed by Hans Bethe[142] in 1944 and later extended by others,[143,150] circumvents

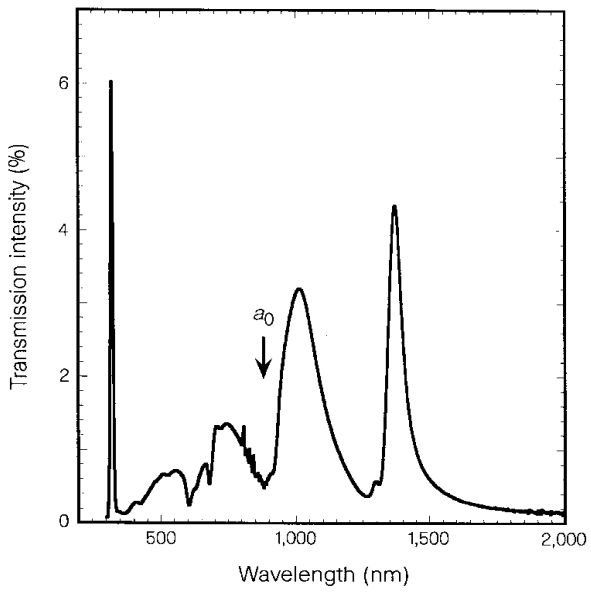

Figure 4.2: EOT spectrum, at normal incidence, from square array of subwavelength holes in Ag film. *Parameters*: periodicity, $a_0 = 900$ nm; hole diameter, $d = 150$ nm; film thickness, $t = 200$ nm; hole coverage, $f \equiv \pi(d/2)^2 \Big/ a_0^2 = 2.2\%$. After Reference [6].

the fundamental inconsistencies in Kirchhoff's formulation of diffraction[116] by treating the transmitted radiation as if originating from two virtual dipoles: an electric dipole normal to the aperture and a magnetic one in the plane of the aperture. This distribution of "fictitious magnetic charges and currents" in the diffracting hole ensures the fulfillment of the boundary conditions on the opaque screen and in the aperture itself. The influence of Bethe's calculation in coining the phrase "extraordinary optical transmission" can be easily appreciated by considering in Figure 4.2 the maximum observed transmission at λ = 1370 nm (neglecting the sharp leftmost peak for now)—about $4.5\%/f$, where f is the areal coverage of the holes—and comparing that to the very weak transmission predicted by the Bethe's theory for an aperture of the same diameter and at the same wavelength. The enhancement factor speaks for itself:

$$\frac{T_{\text{observed per hole}}}{T_{\text{Bethe}}} = \frac{T_{\text{observed}}/f}{\frac{64\pi^2}{27}\left(\frac{d}{\lambda}\right)^4} = \frac{T_{\text{observed}}}{\frac{\pi}{4}\left(\frac{d}{a_0}\right)^2 \times \frac{64\pi^2}{27}\left(\frac{d}{\lambda}\right)^4} = \frac{0.045}{\frac{16\pi^3}{27}\frac{(150\text{ nm})^6}{(900\text{ nm})^2(1370\text{ nm})^4}} \approx 614 \tag{4.1}$$

Transmission enhancements like the one in Equation 4.1 were one of the reasons to call the phenomenon "extraordinary". The other was the peculiar spectral profile of the observed transmission, which typically consists of a series of peaks separated by valleys of low transmission. For instance, the sharp leftmost peak in Figure 4.2 corresponds to the *bulk plasmon* of the silver metal and disappears with increasing film thickness.[6] The bulk or volume plasmon in a metal is the quantum of collective longitudinal oscillations of the conduction electron gas.[61] The energy of the bulk plasmon, characteristic of the given metal, can be calculated from the Drude model for the response of the free-electron gas to an applied electric field, extended to account for the polarizability of the bound electrons by a constant offset (ε_∞) to the dielectric function of the metal[61,112] and leading to an expression for the plasma frequency ω_p (or wavelength λ_p) of the collective oscillation:

$$\omega_\mathrm{p} = \sqrt{\frac{Ne^2}{\varepsilon_\infty \varepsilon_0 m_e^*}}\,, \quad \lambda_\mathrm{p} = \frac{2\pi c}{\omega_\mathrm{p}} \tag{4.2}$$

Substituting in Equation 4.2 for the density[110] ($N = 5.86 \cdot 10^{28}$ m^{-3}) and effective mass ($m_e^* \approx m_e$) of the free electrons in Ag, as well as for the background dielectric constant[151] ($\varepsilon_\infty \approx 6$) and the remaining natural constants ($e = 1.602 \cdot 10^{-19}$ C, $m_e = 9.109 \cdot 10^{-31}$ kg, $c = 3 \cdot 10^{17}$ nm $\cdot$ s^{-1}), yields the theoretical bulk-plasmon wavelength for Ag: $\lambda_\mathrm{p} = 338$ nm. This value matches reasonably well the observed position, 326 nm, of the leftmost peak in Figure 4.2.

However, what really intrigued Ebbesen and colleagues about an EOT spectrum like the one in Figure 4.2—and continues to occupy many researchers a decade since the original EOT report—were the other high-transmission peaks, especially those at wavelengths greater than the array periodicity. Based partly on the lack of extraordinary transmission from a hole array in nonmetallic germanium, and partly on angle-dependent EOT measurements for noble-metal samples, Ebbesen *et al.*[6] attributed the EOT effect to the excitation of *propagating* surface plasmons, which arise from the coupling between optical radiation and the collective longitudinal oscillations of the free-electron charge density at the bound-

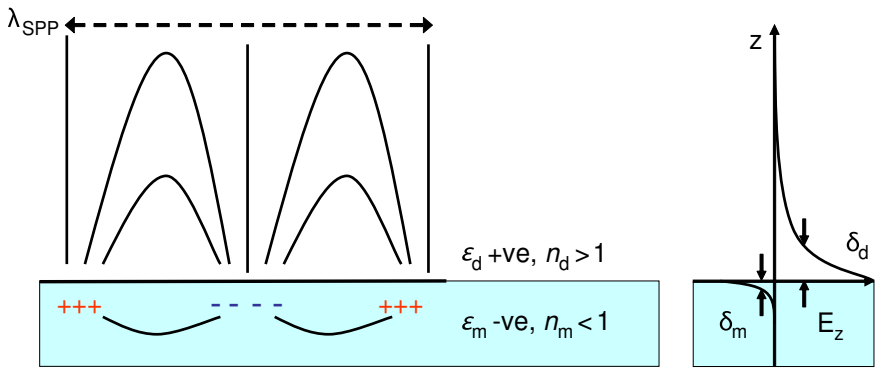

Figure 4.3: Left: Surface-plasmon polaritons (SPPs) at the interface between a metal of relative permittivity ε_{m} and a dielectric of relative permittivity ε_{d} have a combined electromagnetic-wave and surface-charge character, which causes the electric-field component perpendicular to the surface (E_z) to become enhanced near the surface and decay exponentially with away from it. **Right:** The E_z-field is evanescent, reflecting the bound nature of SPPs on a flat surface, so power does not propagate away from the interface. In the dielectric medium above the metal, typically air or glass, the decay length δ_{d} of the field is of the order of the wavelength of the excitation light, whereas the decay length δ_{m} into the metal is determined by the skin depth (*e.g*, about 25 nm for Ag). After Reference [152].

ary between a metal and a dielectric.[153] When an electromagnetic wave impinges on a good metal, it penetrates only a short distance into the material[127] ($\delta_{\mathrm{m}} < 50$ nm for Au or Ag at optical wavelengths) because of the high absorption coefficient, which results in high reflectivity; therefore, only the free electrons very close to the surface can interact with the incident wave. Such interaction of surface electrons with the electric field of the incident light can lead to a collective displacement of the free electrons with respect to the lattice of fixed positive ions and give rise to a charge-density wave propagating across the surface, known as a *surface-plasmon polariton* (SPP) (Figure 4.3a). Conceptually, SPPs can be thought of as "light waves that are trapped on the surface because of their interaction with the free electrons of the conductor".[154]

Surface-plasmon polaritons are surface-bound modes: SPP waves can propagate along the metal-dielectric interface for tens or even hundreds of micrometers for noble metals, limited only by the low Ohmic losses embodied in the imaginary part k''_{SPP} of the SPP

wavevector, but suffer strong attenuation away from the surface (Figure 4.3b). The dispersion relation between the angular frequency ω and the in-plane wavevector k_{SPP} of the surface waves for a flat metal-dielectric interface can be obtained by seeking surface-mode solutions of Maxwell's equations under appropriate boundary conditions. Continuity of the normal component of the displacement field $D_z = \varepsilon E_z$ requires that the real part of the relative permittivity of the metal $\varepsilon'_{\mathrm{m}}$ and the relative permittivity of the dielectric $\varepsilon'_{\mathrm{d}}$ have opposite signs, in order to allow for charges to be sustained at the metal surface.[152] In other words, materials surrounded by dielectrics can support SPP modes only in those spectral regions where $\Re\mathrm{e}\left[\varepsilon_{\mathrm{m}}(\omega)\right] \equiv \varepsilon'_{\mathrm{m}}(\omega) < 0$. The SPP dispersion relation is then derived as:[112,153]

$$k_{\mathrm{SPP}} = \frac{\omega}{c}\sqrt{\frac{\varepsilon_{\mathrm{d}}\varepsilon_{\mathrm{m}}}{\varepsilon_{\mathrm{d}}+\varepsilon_{\mathrm{m}}}}, \quad \text{with} \quad k_{\mathrm{SPP}} \equiv k'_{\mathrm{SPP}} + \mathrm{i}k''_{\mathrm{SPP}} \tag{4.3}$$

The relative permittivity of the metal can be approximated using a Drude-model expression for the frequency dispersion:[112]

$$\varepsilon_{\mathrm{m}}(\omega) \equiv \varepsilon'_{\mathrm{m}}(\omega) + \mathrm{i}\varepsilon''_{\mathrm{m}}(\omega) = 1 - \frac{\omega_{\mathrm{p}}^2}{\omega^2 + \mathrm{i}\Gamma\omega} \tag{4.4}$$

where ω_{p} is the plasma frequency of the metal (Equation 4.2) and Γ is the rate of dissipation of the electron motion through scattering (for silver,[152] $\Gamma_{\mathrm{Ag}} = 1.45 \cdot 10^{-13}$ s^{-1}). For weak damping, $|\varepsilon''_{\mathrm{m}}| \ll |\varepsilon'_{\mathrm{m}}|$, the SPP wavelength λ_{SPP} (Figure 4.3) can be obtained from the real part of the SPP wavevector k'_{SPP}:

$$k'_{\mathrm{SPP}} \approx \frac{\omega}{c}\sqrt{\frac{\varepsilon_{\mathrm{d}}\varepsilon'_{\mathrm{m}}}{\varepsilon_{\mathrm{d}}+\varepsilon'_{\mathrm{m}}}} \quad \Rightarrow \quad \lambda_{\mathrm{SPP}} = \frac{2\pi}{k'_{\mathrm{SPP}}} \approx \lambda\sqrt{\frac{\varepsilon_{\mathrm{d}}+\varepsilon'_{\mathrm{m}}}{\varepsilon_{\mathrm{d}}\varepsilon'_{\mathrm{m}}}} \tag{4.5}$$

where λ is the wavelength of the excitation light in the dielectric medium. In Figure 4.4, the SPP dispersion curve for a flat metal-air interface (solid line), when compared to the light line in air (dotted line), reveals a crucial characteristic of SPPs that reflects their bound nature on a flat, undecorated interface: a wavevector mismatch between the SPP mode and light, that is, the surface-plasmon polariton always carries greater momentum

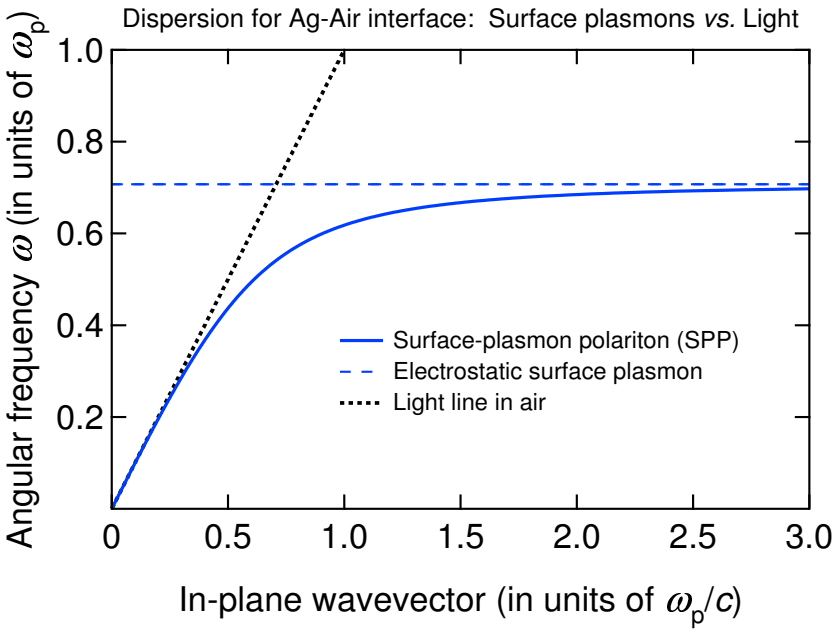

Figure 4.4: Frequency dispersion of SPP wavevector k'_{SPP} at Ag-air interface (see Equation 4.5), with asymptotic SP frequency $\omega_{\mathrm{sp}} = \omega_{\mathrm{p}}/\sqrt{2}$, *vs.* "light line" $k_0 = \omega/c$ in air. Note the wavevector (momentum) mismatch, $k'_{\mathrm{SPP}} > k_0$.

than a free-space (air) photon of the same frequency.[153,154] The physical reason for the increased momentum of the SPP is that the light field has to "drag" the electrons along the metal surface.[112] For large values of the wavevector, the SPP dispersion relation approaches the asymptotic frequency ω_{sp} of the *non-propagating* plasma oscillations at the interface, the electrostatic *surface plasmon* (SP): $\omega_{\mathrm{sp}} = \omega_{\mathrm{p}}/\sqrt{1+\varepsilon_{\mathrm{d}}}$. At the opposite limit of small wavevectors, SPPs are more "light-like", hence the designation "polaritons". Nevertheless, light of any frequency impinging from a dielectric medium onto a flat metal surface cannot directly excite the SPP modes at the same interface, unless the missing wavevector mismatch is somehow compensated. This is precisely where the periodic structuring of a hole array begins to shine.

According to the model of SPP-mediated EOT, the periodic surface structure of the hole array serves a triple purpose (Figure 4.5): **(i)** coupling of the incident light into surface-plasmon excitations, via scattering/diffraction at the input interface, to produce bound

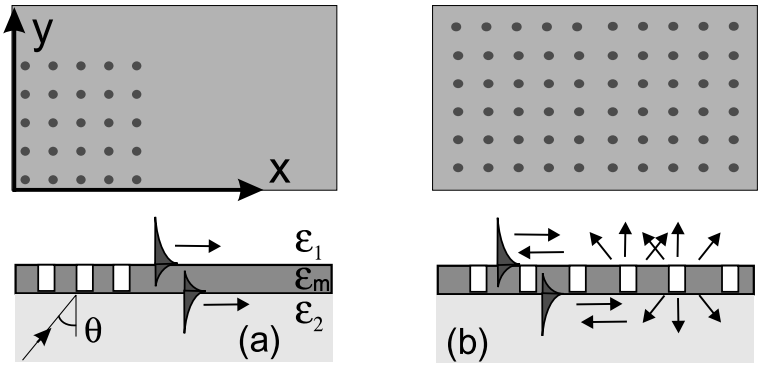

Figure 4.5: Schematics of light-SPP-light coupling. **(a)** SPP excitation by diffraction of incident light from perforated surface region and subsequent surface-bound propagation on smooth region; **(b)** SPP excitation, propagation, interference, and eventual scattering back into light from perforated surface region. After Reference [155].

SPP modes; **(ii)** selecting the wavelengths of allowed SPP modes via SPP-SPP interference; and **(iii)** scattering/diffraction of the bound SPPs at the output interface into propagating light, whose zeroth diffraction order becomes the observed transmission.[155] For a structured metal film bounded by dielectrics, light readily interacts with the surface charges because the structure can bridge the photon-SPP momentum gap through scattering/diffraction (Figure 4.5). Conservation of momentum for a square-lattice hole array of periodicity a_0 takes the following form:[155,156]

$$\vec{\mathrm{k}}_{\mathrm{SPP}} = \vec{\mathrm{k}}_{xy} \pm p\vec{\mathrm{G}}_x \pm q\vec{\mathrm{G}}_y \ , \quad \text{with} \tag{4.6}$$

$$\vec{\mathrm{k}}_{xy} = \hat{\mathrm{u}}_{xy}\sqrt{\varepsilon_{\mathrm{d}}}\left(\frac{\omega}{c}\right)\sin\theta \quad \text{and} \quad \left|\vec{\mathrm{G}}_x\right| = \left|\vec{\mathrm{G}}_y\right| \equiv \frac{2\pi}{a_0} \tag{4.7}$$

where $\hat{\mathrm{u}}_{xy}$ is the unit vector in the direction of the in-plane wavevector k_{xy} of the light of frequency ω incident at an angle θ; $\varepsilon_{\mathrm{d}} = \{\varepsilon_1,\ \varepsilon_2\}$ is the relative permittivity of either dielectric medium; pG_x and pG_y are the magnitudes of the reciprocal-lattice vectors, with integers $(p,\ q)$ designating the different SPP modes. At normal incidence ($\theta = 0°$), combining Equations 4.5 and 4.6 yields a first approximation for the spectral positions $\lambda_{\max}$ of

the EOT peaks:

$$\lambda_{\max}(p,\ q) \approx \frac{a_0}{\sqrt{p^2+q^2}} \sqrt{\frac{\varepsilon_{\mathrm{d}}\varepsilon'_{\mathrm{m}}}{\varepsilon_{\mathrm{d}}+\varepsilon'_{\mathrm{m}}}} \tag{4.8}$$

Figure 4.6 illustrates the use of Equation 4.8 for peak designation, whereby transmission peaks are attributed to different SPP modes corresponding to different substrates and four-fold degenerate $(\pm p,\ \pm q)$ pairs.[7] The peak widths, although partly due to inhomogeneous broadening from irregularities in the holes,[7] are mostly governed by the lifetime of the SPP modes before they scatter back into light.[157]

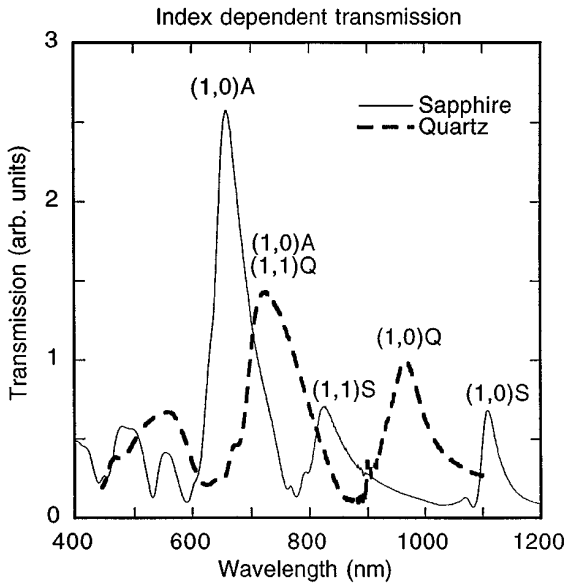

Figure 4.6: Peak designation according to SPP model for experimental EOT spectra of perforated Ag films on quartz (Q) and sapphire (S) substrates, with air (A) on opposite side. *Parameters*: $a_0 = 600$ nm, $d = 150$ nm. After Reference [7].

Matching the resonant wavelengths on both sides of a perforated metal film presents one way to control the EOT effect.[146] In general, two sets of resonances appear in the transmission spectra because each surface of the hole array borders on a different dielectric, typically the solid substrate and air, each with a different permittivity ε_{d}. Replacing air, for instance, with various index-matching liquids allows for tuning of the transmission

spectra, as varying the dielectric environment on one side of the structure influences the SPPs associated with both interfaces. The apparent coupling between the two interfaces is a form of evanescent Fabry-Perot resonances that re-circulate energy inside the holes and thus serve to amplify to an "extraordinary" extent the inherently weak transmission in the sub-wavelength regime, where cylindrical cavities cannot sustain propagating modes.[146,158–160] A key result of this resonant interaction is that minimizing the energy difference between SPP modes on opposite sides of the perforated metal film maximizes the peak transmission intensity (Figure 4.7); numerical simulations also confirm the experimental observations.[146] Therefore, within the framework of the surface-plasmon model, the EOT effect arises owing to a combination of SPP resonances at either or both interfaces and evanescent Fabry-Perot resonances inside the holes.[158]

Many authors[146,156,161–164] have elaborated on the initial explanation given by Ebbesen *et al.*[6] that the excitation of surface-plasmon polaritons at either or both metal-dielectric interfaces mediates the EOT effect. A small group of researchers had previously dismissed the role of SPPs and put forth a model of non-resonant generation and interference of composite diffracted evanescent waves (CDEWs);[165] however, a recent exchange of articles,[166–170] comments,[171,172] and responses to comments[173,174] between proponents of the SPP and CDEW models has led to a tacit consensus that surface plasmons must be involved in the extraordinary transmission at visible and near-infrared wavelengths. Although most workers in this field now regard the excitation of SPP modes as the dominant mechanism for mediating the EOT effect, some very recent theoretical work[144] has given further evidence of another contribution to the EOT, namely a "quasi-cylindrical wave creeping along the interface over several wavelength distances"; in fact, in the thermal-IR region, where SPPs are only weakly excited by the array of holes, the cylindrical wave dominates the scattering process.[144] Moreover, other recent studies[158,175] have also identified an additional plasmonic contribution to the observed transmission: the *localized surface-plasmon resonances*[153] (LSPRs) that originate on the metallic ridge of each aperture. Revealing

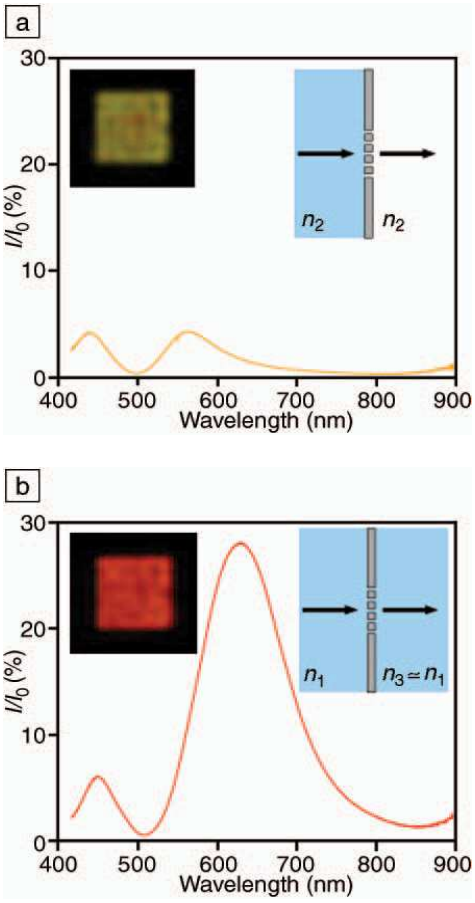

Figure 4.7: EOT effect in asymmetric *vs.* symmetric dielectric environment. Transmission spectra and **(left insets)** optical images of the same hole array in Ag film on quartz substrate ($n_1 \equiv \sqrt{\varepsilon_1} = 1.46$), with **(a)** air ($n_2 = 1$) and **(b)** glycerol ($n_3 = 1.47 \approx n_1$) as the output-side dielectric. *Parameters*: $t_{\mathrm{Ag}} = 200$ nm, $a_0 = 250$ nm, $d = 130$ nm. After Reference [8].

the role of LSPRs in the EOT phenomenon may also help to explain why hole arrays in good metals such as Ag and Au invariably exhibit the largest EOT effects.[175] Other researchers[176–178] interpret the EOT effect in a purely phenomenological fashion—in terms of Fano-type spectral profiles that result from the interference of two distinct contributions: a resonant channel (*e.g.*, SPPs and/or other surface modes) and non-resonant scattering—and account for the observed spectral shapes without explicitly specifying the nature of the resonant channel.

4.2 Experimental details

The nanostructures investigated in this work were: **(i)** hole array in a plain VO_2 film (Figure 4.8a); **(ii)** hole arrays in Au-on-VO_2 and Ag-on-VO_2 double layers (Figure 4.8b); **(iii)** plain VO_2 film. All the VO_2 layers were prepared simultaneously on fused-silica ("glass") substrates in a pulsed-laser deposition system (PLD: KrF excimer laser at $\lambda =$ 248 nm, fluence ≈ 4 J·cm^{-2}) by ablating a V-metal target in a 12-mtorr O_2 atmosphere at 550 °C. The resulting film thickness was 200 nm, as determined by Rutherford backscattering spectrometry (RBS). The Ag and Au overlayers were deposited in a bell-jar thermal evaporator. The RBS-measured thickness was 160 nm for Ag and 230 nm for Au. The hole arrays, consisting of 60-by-60 circular apertures of 250-nm nominal diameter and 750-nm pitch, were milled down to the substrates using a focused ion beam (FIB: 30-keV Ga^+, 90-pA beam current). Figure 4.9 shows a FIB micrograph of the VO_2 array (structure (i) above), while Figure 4.8c shows a portion of the same array imaged in transmission with a scanning near-field optical microscope (SNOM: $\lambda = 532$ nm, aperture ≈ 100 nm); a schematic of the SNOM setup is given in Figure 4.10a. We note here that the air-filled holes in the SNOM image of the VO_2 hole array (Figure 4.8c) appear darker—that is, transmit less—than the surrounding VO_2 film, whereas the contrast is reversed in the case of holes in Ag-VO_2 (Figure 4.8d) or Au-VO_2 (not shown) double-layer hole arrays. We shall return to this observation shortly. Spectral measurements at normal and oblique incidence were performed using nearly collimated white light delivered through a multimode optic fiber to a stopped-down micro-objective (Figure 4.10b). The incident-beam spot was slightly smaller than the size of the array, with a beam divergence of about $\pm 1^o$. The transmission spectrum through each sample was collected in the zero-diffraction-order (*i.e.*, detected beam collinear with incident beam) by another micro-objective, stopped down to reduce outgoing-beam divergence to about $\pm 1^o$, and coupled to another multimode fiber. The fiber was fed into a spectrometer equipped with a cooled charge-coupled-device (CCD) detector. The substrates were attached to a resistor-heated sample holder, mounted on a

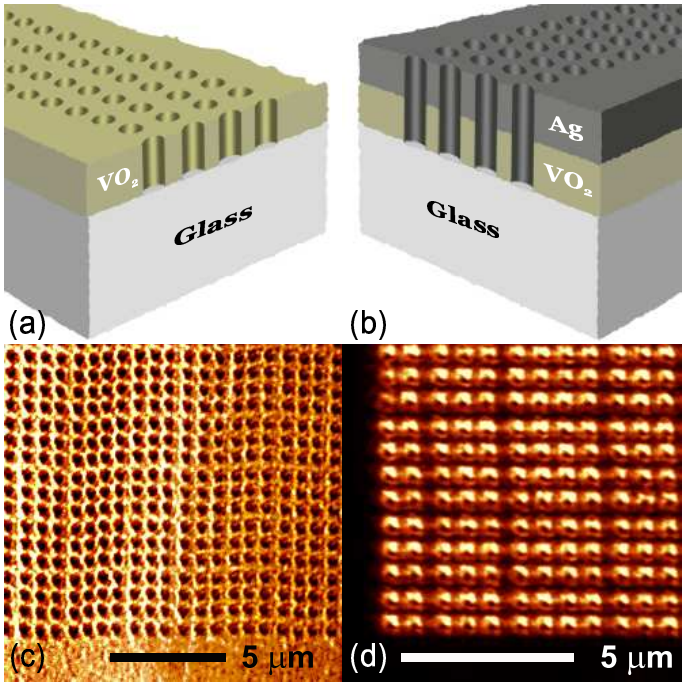

Figure 4.8: Schematics of hole arrays in **(a)** single VO_2 layer and **(b)** Ag/Au-VO_2 double layers. SNOM transmission images (λ = 532 nm) of hole arrays in: **(c)** single layer of VO_2 (semiconducting phase) and **(d)** Ag-VO_2 double layer. All nanostructures are on fused-silica ("glass") substrates.

translation-rotation stage, with a precision thermocouple placed in contact with the top surface of the sample. The position of the hole array with respect to the incident-beam spot was monitored in reflection via a CCD camera connected to a video display.

4.3 Results and discussion

4.3.1 Periodic double-layer hole arrays: EOT modulation and reverse hysteresis

Figure 4.11 presents the main experimental results of our work in Reference [125]: **(i)** controlled switching of the EOT effect through periodic arrays of subwavelength holes via the temperature-induced metal-semiconductor transition of VO_2; and **(ii)** counterintuitive transmission behavior of the VO_2 layer in these nanostructures. Figure 4.11a shows the transmission spectra for a hole array in a silver-VO_2 double layer on glass, at two different temperatures that correspond to the two phases of the VO_2 layer. It is immediately obvi-

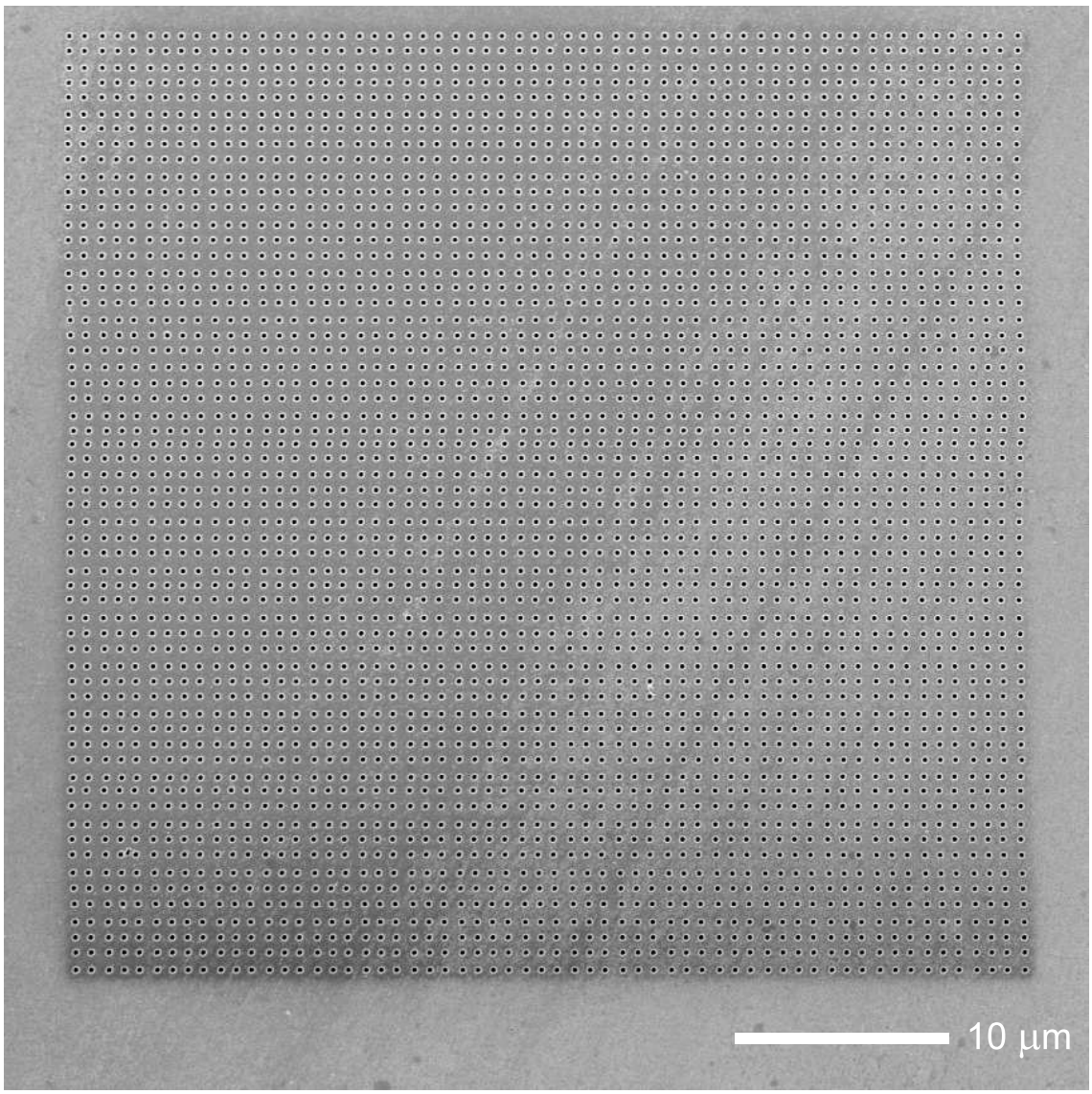

Figure 4.9: FIB micrograph of periodic array of 3600 circular holes in single layer of VO_2 on glass. *Parameters*: $d = 250$ nm, $a_0 = 750$ nm, $t_{VO_2} = 200$ nm.

ous that, for wavelengths greater than about 600 nm, the high-temperature, metallic-phase transmission dominates. The transmission contrast in the visible range is rather small, at some points even slightly in favor of the low-temperature, semiconducting-phase transmission, since the optical properties of the two VO_2 phases only begin to differ significantly in the near-IR range, as evidenced by the spectral dependence of the complex permittivity (Figure 4.1a) and transmission (Figure 4.1b). Figure 4.12a shows the EOT intensity for the

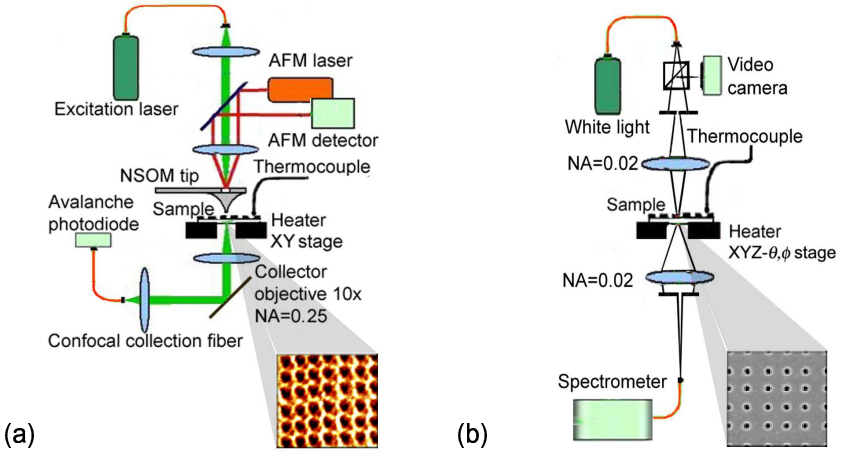

Figure 4.10: Schematics of **(a)** SNOM setup and **(b)** optical setup for transmission spectra.

Ag-VO_2 hole array as a function of temperature at a wavelength of 800 nm. Comparing the shape of this hysteresis curve to that of a plain VO_2 film (Figure 4.12b), it becomes clear why we call our observation *reverse switching* of VO_2. As explained later on, it is the permittivity contrast between the content of the holes (air) and the surrounding material (VO_2) that brings about this effect.

The controlled switching of EOT in the near-IR range stands out even more prominently in the case of a perforated gold-VO_2 double layer on glass (Figure 4.11b)—for example, the high-temperature, metallic-phase transmission at 800 nm exceeds the low-temperature, semiconducting-phase transmission by an order of magnitude. The magnitude of the EOT effect through the gold-VO_2 hole array is smaller than the magnitude in the corresponding phase of the silver-VO_2 nanostructure, partly because of the larger metal-layer thickness[179] and smaller hole diameter[180] for the gold-VO_2 structure, and partly due to gold being more dissipative than silver. The relative sharpness of the maximum transmission peak for the Au-VO_2 structure may also be related to hole size: Smaller holes, being less efficient scatterers of surface modes into far-field light, diminish the radiative damping and hence increase the lifetime of these modes, which in turn reduces the width of the peak.[157] Overall, the key observation holds for both types of structures, namely that EOT in the metallic

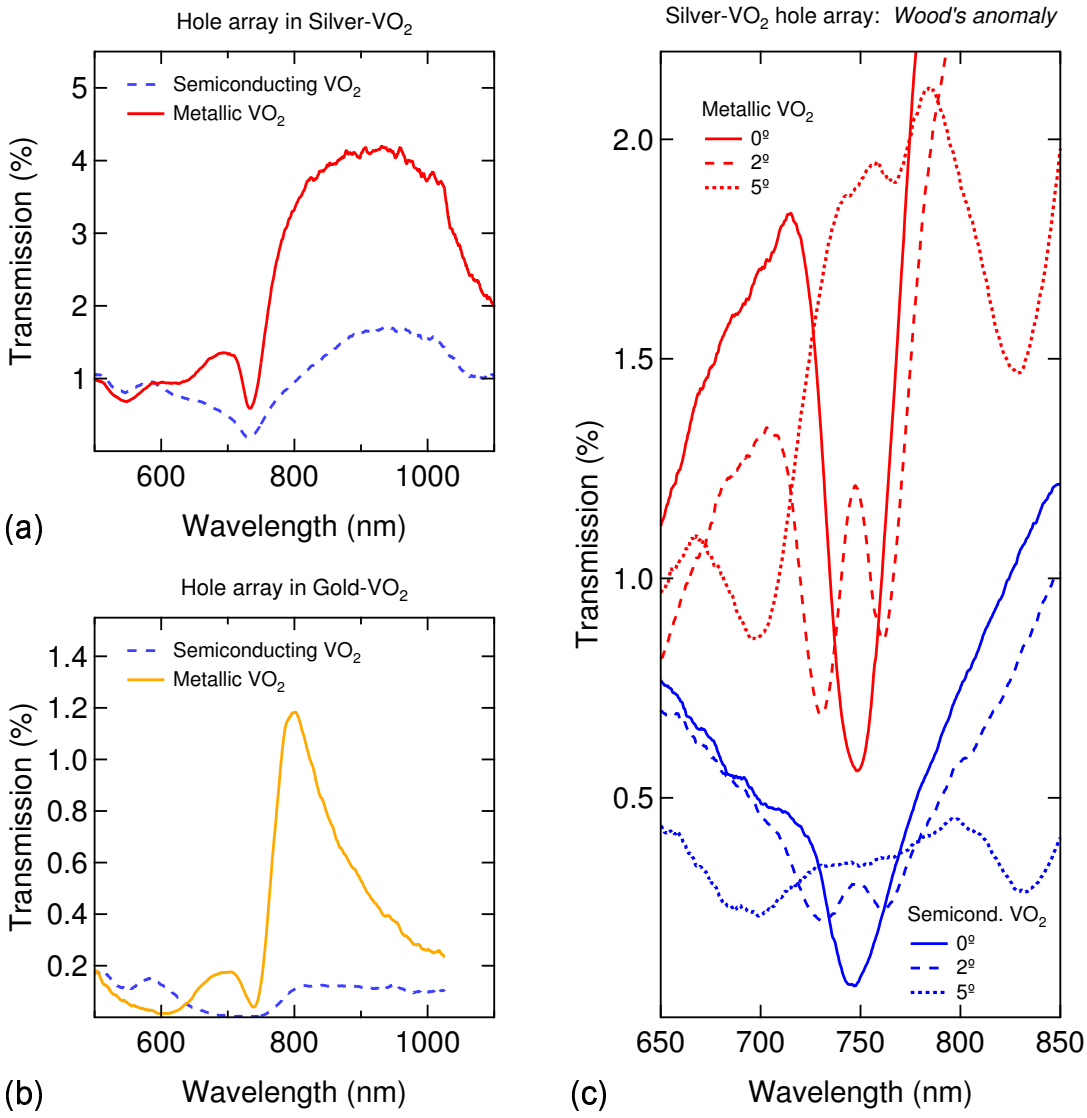

Figure 4.11: Experimental zero-order, normal-incidence transmission spectra for periodic hole arrays in **(a)** Ag-VO_2 and **(b)** Au-VO_2, in each phase of the VO_2 layer. **(c)** Demonstration of spectral splitting of Wood's anomaly minima with deviation from the normal (0^o) angle of incidence (lower/upper set of three curves corresponds to the semiconducting/metallic phase of the VO_2 layer in the Ag-VO_2 nanostructure). Note the *reverse switching* trend, whereby transmission is higher in the metallic phase of the VO_2 layer, contrary to the regular switching of a plain VO_2 film of the same thickness.

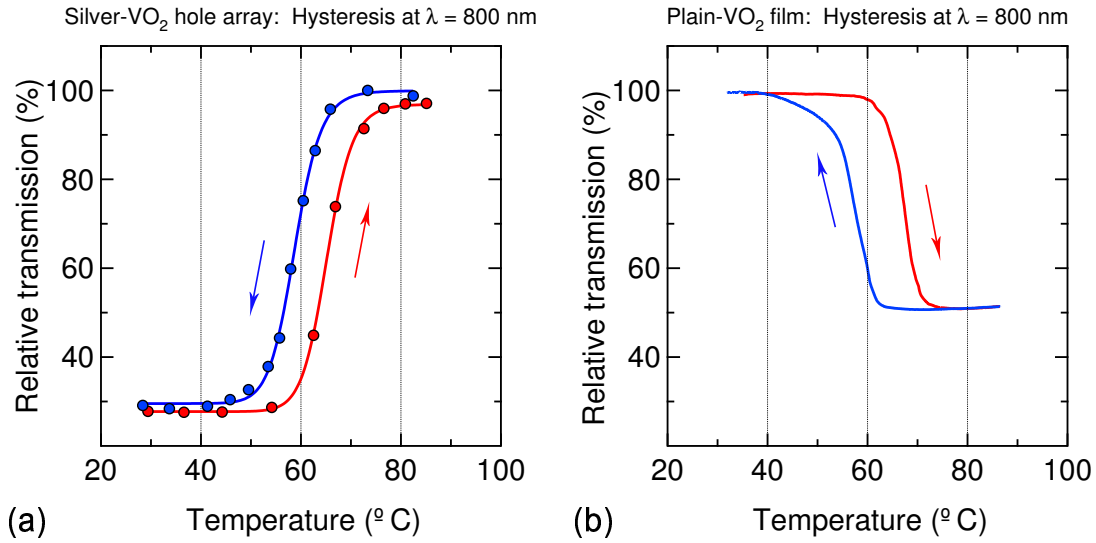

Figure 4.12: **(a)** *Reverse hysteresis* for periodic Ag-VO_2 hole array, normalized to highest transmission in metallic phase of VO_2 layer; upward/downward arrow denotes heating/cooling branch of thermal cycle. **(b)** *Regular hysteresis* for plain VO_2 film, normalized to highest transmission in semiconducting phase; downward/upward arrow denotes heating/cooling branch of thermal cycle.

phase of VO_2 is enhanced over EOT in the semiconducting phase.

Most EOT spectra exhibit sharp minima in the transmission profile, usually preceding the transmission peaks. These minima have routinely been attributed to the so-called *Wood's anomaly* for diffraction gratings,[181] which amounts to the disappearance of a diffracted order as it becomes tangent to the plane of the grating, caused by the accumulation of in-phase scattering events.[182] The spectral positions of the minima are also known as Rayleigh wavelengths. At normal incidence, the first-order Rayleigh wavelength (λ_R) coincides with the grating spacing,[183] that is, with the periodicity of the array. The sharp normal-incidence minima for our samples occur close to 750 nm (Figure 4.11a and 4.11b), which corresponds to the nominal lattice spacing of the hole arrays. As the angle of incidence is increased, the Rayleigh wavelengths for grazing orders should become longer on one side of the sample normal and shorter on the other side.[183] Consequently, we expect the sharp minimum at λ_R to split into two separate minima: one occurring at $\lambda_{R-} < \lambda_R$ and the other at $\lambda_{R+} > \lambda_R$. The experimental observations confirm this prediction. Figure

4.11c shows the splitting of the normal-incidence Wood's anomaly as the sample plane is rotated with respect to the optic axis. The incident light was polarized with the electric field oscillating parallel to the rows of the Ag-VO_2 hole array. Both VO_2 phases exhibit two sharp dips in each of their transmission curves for nonzero angles of incidence (θ_{inc}): for instance, the zero-order transmission at $\theta_{\text{inc}} = 2^{\text{o}}$ has one dip at 730 nm and another at 760 nm, as opposed to the single dip at 750 nm for zero-order transmission at $\theta_{\text{inc}} = 0^{\text{o}}$. In addition, we find once again that EOT in the metallic state of the VO_2 layer exceeds, for all pairs of curves, EOT in the semiconducting state.

4.3.2 Numerical simulations

Numerical simulations of the relevant optical quantities (transmission, reflection, scattering) were undertaken to gain some insight into the origin of the observed reverse switching of the EOT effect. The simulated zero-order transmission spectra for perforated Ag-VO_2 and Au-VO_2 structures are given in Figure 4.13, and those for a perforated single layer of VO_2 (see Section 4.3.4) are given in Figure 4.14(c, d).

The computational scheme used here stems from a numerical method for modelling the properties of patterned photonic crystal slabs, and is described in the work of Tikhodeev *et al.*[149] We also used the complex frequency-dependent permittivity of VO_2 from Reference [57] (Figure 4.1a), and those of Ag and Au from Reference [184]. The *transfer-matrix formalism* employed in the simulations contains the following basic elements:[149] **(i)** in-plane periodicity of the hole array is represented as a Fourier decomposition of the piecewise complex permittivity within each layer in terms of reciprocal square-lattice vectors; **(ii)** the solution of Maxwell's equations in each layer is decomposed into sets of eigenvectors propagating in both directions along the normal to the surface of the structure; **(iii)** *transfer matrices* connect the amplitudes of partial waves at different planar slices of the structure inside the same layer; **(iv)** *interface matrices* connect the partial-wave amplitudes across successive layers of the structure (*e.g.*, crossing from Au into VO_2) by imposing continuity

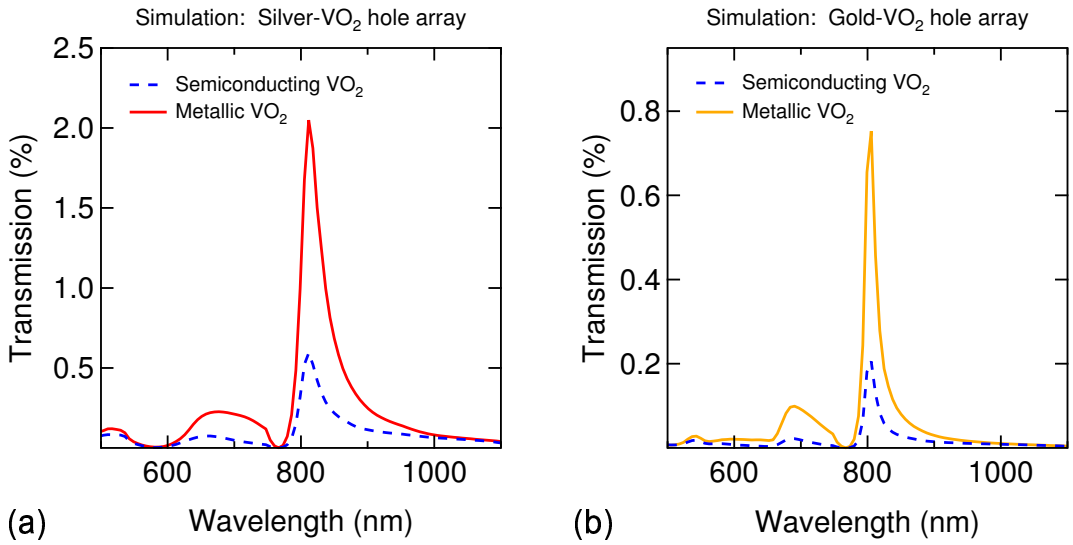

Figure 4.13: Numerical simulations of zero-order, normal-incidence transmission spectra for periodically perforated **(a)** Ag-VO_2 and **(b)** Au-VO_2 double layers on glass, in each phase of the VO_2 layer. The simulated spectra also exhibit the surprising trend of *reverse switching* of VO_2 observed in the experiments.

conditions on the in-plane components of the electric and magnetic fields at the interface; **(v)** *material matrices* convert the partial-wave amplitudes at a given point into in-plane components of electric and magnetic fields at that point. In essence, the goal is to construct a *total transfer matrix* that connects the field amplitudes at different dielectric planes. From knowledge of the total transfer matrix at a given frequency of the incoming light, the reflection, transmission, scattering, and absorption can be computed from the output electromagnetic field components; the computation is then repeated throughout the spectral range of interest.

Despite several simplifications to the model, such as square instead of circular apertures, infinite instead of finite arrays, and a limited number of Fourier components used in representing the in-plane dielectric variation, the simulation results show reasonable qualitative agreement with the corresponding experimental findings. Crucially, the simulations corroborate the key experimental observation of this work, namely, that EOT through perforated Ag-VO_2 and Au-VO_2 nanostructures receives a further enhancement in the near-IR range

when the VO_2 layer becomes metallic. Even though the simulated spectra differ in shape and absolute magnitude from the corresponding experimental curves, they unequivocally demonstrate the effect of *reverse switching* of VO_2.

4.3.3 Why is transmission higher in the metallic phase?

Regarding the reverse-switching effect, we propose the following heuristic explanation. Since the Ag and Au films are optically thick, the incident light cannot traverse the non-perforated areas in the metal-VO_2 hole arrays, as evidenced, for example, by the black regions in Figure 4.8d. Therefore, transmission can only occur through the holes in the metal layer, in the form of evanescent waves generated by diffraction of the incident light at the metal-air interface and mediated mostly by SPPs. The waves emanating from the holes in the metal overlayer undergo additional scattering at the metal-VO_2 interface and must then travel through the perforated VO_2 layer, where they become *leaky evanescent waves*, that is, surface-bound waves that lose intensity as they propagate.[108] The VO_2 material acts as a lossy medium: The evanescent waves penetrate the side walls of the air-filled holes and "leak" into the plane of the VO_2 layer, where partial absorption occurs. As a result, the leakage channels a portion of the light away from the zero-order transmission path and thus renders it undetected in the far field. As discussed in Section 4.3.4 below, the amount of light that penetrates into the VO_2 material between the holes evidently depends on the optical constants of metallic or semiconducting VO_2 and, in particular, on the permittivity contrast between the hole content (air) and its surroundings (VO_2). Besides mitigating the leakage of evanescent waves into the VO_2 layer, a lower permittivity contrast also seems to reduce the diffuse scattering from the holes at the air and glass interfaces;[185] conversely, higher permittivity contrast increases those losses. In the near-IR wavelength range, the permittivity of metallic VO_2 differs considerably from its semiconducting counterpart (Figure 4.1a): at $\lambda = 850$ nm, for example, $\tilde{\varepsilon}\{VO_2{-}\text{met.}\} = 2.67 + 2.98\text{i}$, while $\tilde{\varepsilon}\{VO_2{-}\text{semi.}\} = 8.17 + 2.65\text{i}$. Therefore, because the permittivity contrast between the

air interior and the VO_2 exterior of the holes is lower in the case of metallic VO_2, the high-temperature EOT receives an enhancement over the low-temperature EOT.

4.3.4 Periodic single-layer hole array: Role of perforated VO_2

In order to bring out the significance of the VO_2 layer for the metallic-phase enhancement of EOT in the Ag-VO_2 and Au-VO_2 hole arrays, we also examined the optical properties of a hole array in a single VO_2 film on glass (Figure 4.8a), that is, without a noble-metal overlayer, as described in our Reference [124]. It must be noted that transmission observed through this type of structure is not *extraordinary* in the sense used thus far, owing to the insufficient opacity of the VO_2 layer for direct transmission and its inability to support SPP modes in the wavelength region of interest, since $\Re\mathrm{e}\,[\tilde{\varepsilon}_{\mathrm{met.}}(\lambda < 1.2\ \mu\mathrm{m})] > 0$ (Figure 4.1a).

Figure 4.14a compares the zero-order transmission of a hole array and a non-perforated (plain) area nearby, in the *semiconducting phase* of the same VO_2 film. The hole array transmits less than the intact film throughout the wavelength range because the array diffracts some of the incident intensity away from the detector path, which then cannot contribute to the zero-order transmission. Similarly to the loss mechanisms discussed above (Section 4.3.3), a portion of the diffracted field becomes trapped as leaky waves in the plane of the VO_2 layer, while some of the light that persists in the zero order inside the holes undergoes additional diffuse scattering at the glass interface. Also, since direct transmission through the partially transparent VO_2 film overwhelms the transmission emerging from the holes, the exit apertures appear darker than their surroundings in the aforementioned SNOM image of semiconducting-phase transmission through the VO_2 array (Figure 4.8c).

Figure 4.14b presents the corresponding transmission curves for the *metallic phase* of the VO_2 layer. Here, something intriguing happens in the near-IR range: Despite diffraction/scattering, the zero-order transmission through the hole array exceeds the direct transmission through the plain film. This subtle observation prompted further exploration of the optical behavior of perforated VO_2.

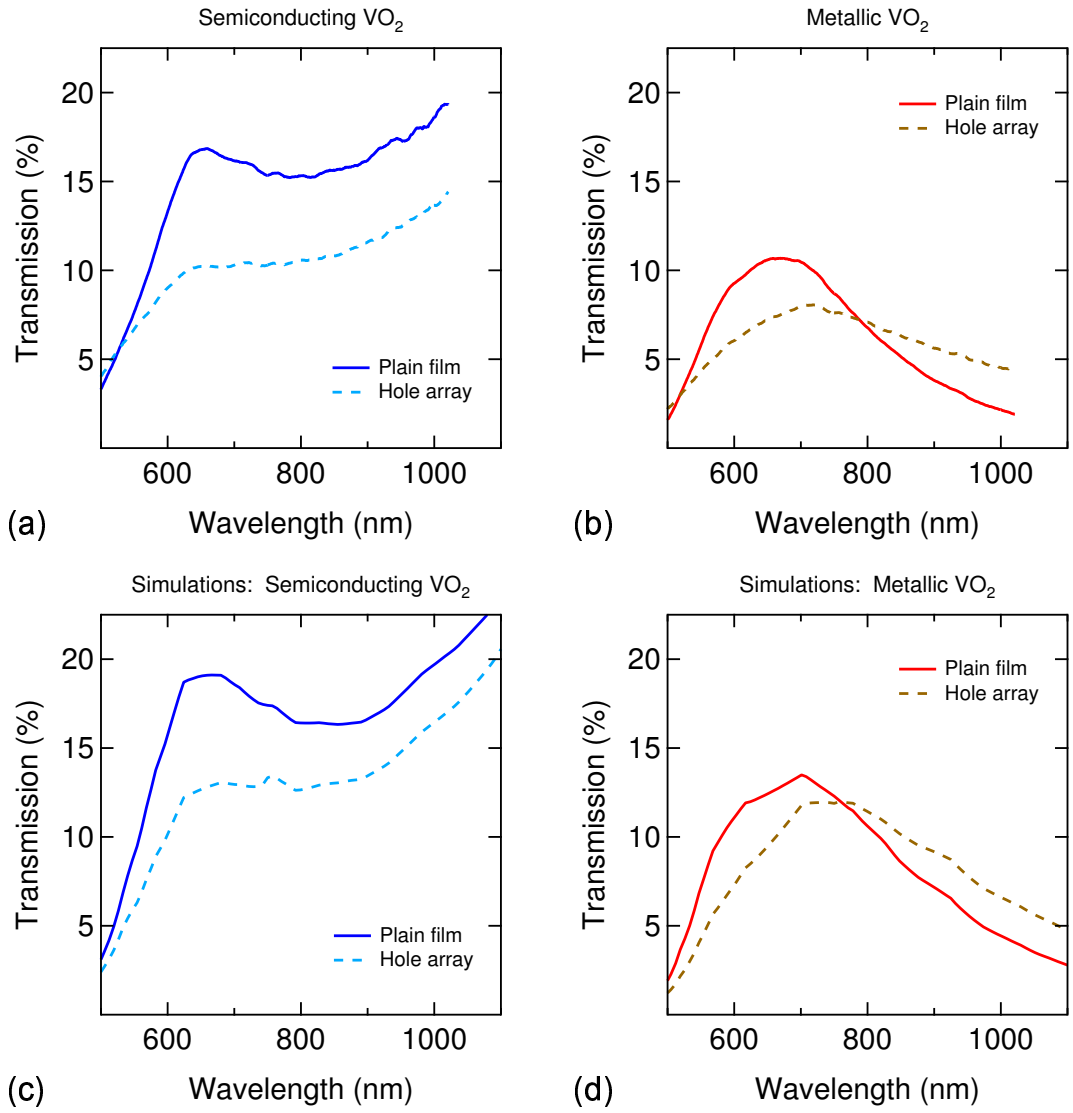

Figure 4.14: **(a, b)** Experimental and **(c, d)** simulated zero-order transmission spectra for plain and periodically perforated single layer of **(a, c)** semiconducting and **(b, d)** metallic VO_2 on glass. Note the crossover region in the metallic-phase spectra.

Using the numerical technique described earlier (Section 4.3.2), we also performed simulations of transmission, reflection, scattering, and absorption for a perforated as well as plain VO_2 film. The zero-order transmission spectra are shown in Figure 4.14c for the semiconducting phase and 4.14d for the metallic phase of the VO_2 film. The simulations reproduce the experimental data quite well; in particular, the simulated curves for the metallic phase show the characteristic crossover in the near-IR region, where the perforated

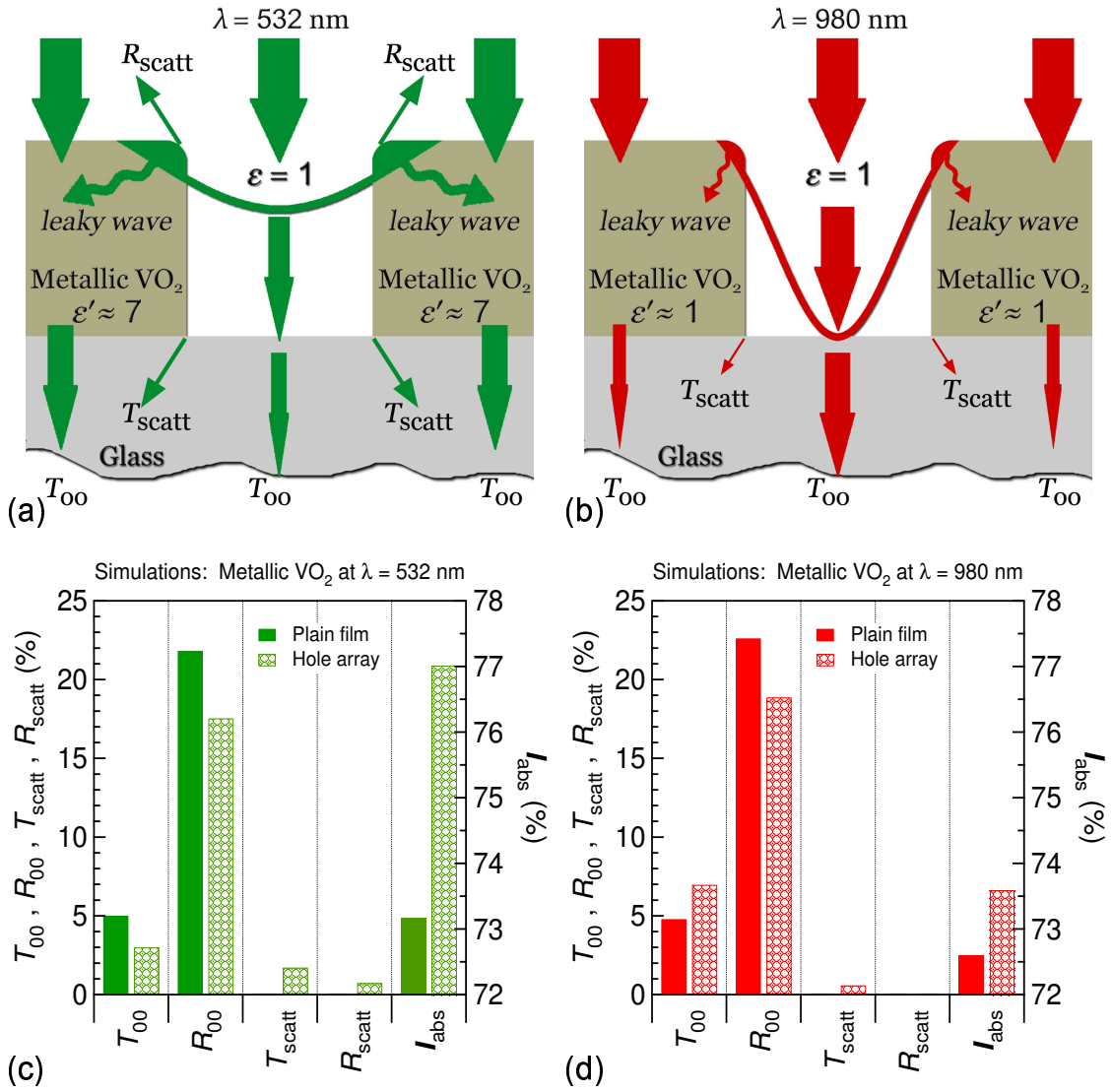

Figure 4.15: Schematics of **(a)** green (λ = 532 nm) and **(b)** near-IR (λ = 980 nm) light propagation through a hole in metallic-phase VO_2 film on glass. Simulated optical quantities for perforated (hatched bars) and plain (solid bars) metallic-phase VO_2 film for **(c)** green and **(d)** near-IR light. According to our model, lower dielectric contrast between the interior (air, $\varepsilon = 1$) and exterior (VO_2, $\varepsilon' \approx 1$) of each hole for metallic VO_2 in the near-IR range reduces the losses from leaky-waves absorption (part of I_{abs}) and diffuse scattering ($T_{\text{scatt}} + R_{\text{scatt}}$), to the extent that T_{00} through the array exceeds T_{00} through the film (direct transmission). *Legend*: $T_{00} \equiv$ zero-order transmission; $R_{00} \equiv$ specular reflection; $T_{\text{scatt}} \equiv$ forward diffuse scattering; $R_{\text{scatt}} \equiv$ backward diffuse scattering; $I_{\text{abs}} \equiv$ absorption (right-side scale) = $100\% - T_{00} - R_{00} - T_{\text{scatt}} - R_{\text{scatt}}$.

VO_2 film transmits more per unit area than the plain film. In fact, it was these simulations for perforated *vs.* plain VO_2 that led us to the explanation (Section 4.3.3) that the reverse switching of the EOT effect results from the permittivity contrast ($\Delta\varepsilon$) between the air-filled hole interiors and the surrounding VO_2 material, which differs considerably not only for the two VO_2 phases but also for different wavelengths in the metallic phase alone (Figure 4.1a).

Thus, higher $\Delta\varepsilon$ brings relatively large losses due to scattering ($T_{\text{scatt}} + R_{\text{scatt}}$) from the apertures[185] and leakage of evanescent waves[108] into the plane of the VO_2 layer (part of I_{abs}), as depicted schematically in Figure 4.15a for metallic-phase VO_2 at a visible wavelength (λ = 532 nm). Conversely, lower $\Delta\varepsilon$ reduces these losses—hence the smaller leaky-wave and scattering arrows in Figure 4.15b, which refers again to metallic-phase VO_2 but at a near-IR wavelength (λ = 980 nm). Therefore, when surrounded by a material of similar real-part permittivity, such as metallic VO_2 in the near-IR, the air-filled holes tend to "funnel" light along the forward direction by reducing the losses due to undetected components of the total optical field, namely leaky waves and diffuse scattering, all to the benefit of the detected zero-order transmission (T_{00}). Furthermore, in comparison with the plain film, the hole array experiences smaller specular reflection (R_{00}) and smaller *direct* absorption (the rest of I_{abs}) in either phase, since a portion of the incident light encounters apertures instead of VO_2 material. Ultimately, when the scattering and absorption losses for the hole array have decreased enough with respect to those for the plain film, T_{00} through the holes prevails over T_{00} through the non-perforated area of the film, and a crossover occurs in the transmission spectra (Figure 4.14(b, d)).

The relative magnitudes of T_{00}, R_{00}, T_{scatt}, R_{scatt}, and I_{abs} (right-side vertical axes) are charted in Figure 4.15(c, d) for plain and perforated VO_2 in the metallic phase, each at the visible and near-IR wavelengths mentioned above. As also noted above, R_{00} for the plain film exceeds R_{00} for the hole array. Conversely, I_{abs} for the array is appreciably greater than I_{abs} for the plain film at the visible wavelength (Figure 4.15c), while in the near-IR the

two absorption magnitudes are very similar (Figure 4.15d) because the effect of the leaky waves is reduced. In the latter case, since the plain film reflects specularly (R_{00}) more than the hole array and since the total diffuse scattering of the array is rather small (T_{scatt} only, as $R_{\text{scatt}} = 0$ for $\lambda \geq 750$ nm), conservation of energy requires that the hole array transmit *more* in the zero order than the plain film (cf, T_{00} bars in Figure 4.15d).

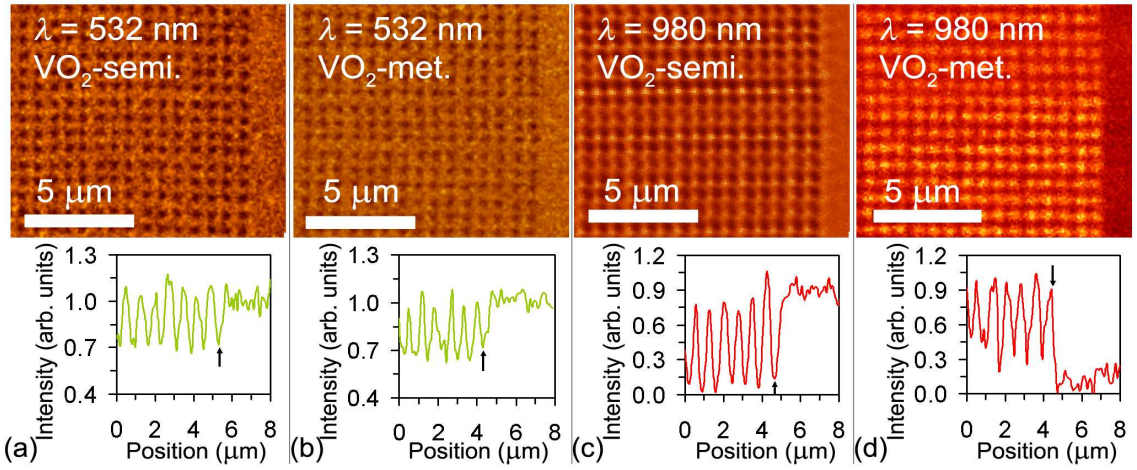

Figure 4.16: Top half: SNOM images of far-field transmission through VO_2 hole array under near-field illumination with **(a, b)** green (λ = 532 nm) and **(c, d)** near-IR (λ = 980 nm) laser, during **(a, c)** semiconducting and **(b, d)** metallic phase of VO_2. **Bottom half:** For each image above, plot of intensity as a function of position along part of a row of holes and extending into non-perforated area; rightmost hole indicated by arrow in each plot. Note that it is only in **(d)** that the holes "light up", that is, transmit more than the surrounding areas.

Perhaps most revealing of all are the SNOM image scans (Figure 4.16) of far-field transmission through individual holes and non-perforated areas, obtained under near-field incident illumination with green (λ = 532 nm) and near-IR (λ = 980 nm) laser light. Below each image in Figure 4.16 is a plot of the detected intensity along part of a row of apertures and extending outside the array into the plain, non-perforated film. The relative position of the rightmost aperture is marked by an arrow in each plot. For *semiconducting* VO_2 (Figure 4.16(a, c)), the intensity reaches local minima within the apertures relative to the intensity

through the plain film, indicating a leakage path through the film at both wavelengths. These observations corroborate the spectral measurements and simulations of T_{00} for semiconducting VO_2 (Figure 4.14(a, c)) by demonstrating that the air-filled holes transmit *less* than the plain film for both visible and near-IR illumination. For *metallic* VO_2, the holes transmit less than the surrounding film only under visible-light illumination (Figure 4.16b). In the near-IR range, however, the intensity contrast is reversed, so that more light emerges from each hole than from an equal-area spot on the intact film (4.16d). The overall effect of this behavior manifests itself in the transmission spectra for metallic-phase VO_2, discussed earlier in reference to Figure 4.14(b, d), where the crossover signifies that T_{00} through the hole array exceeds the direct transmission through a non-perforated area of the film.

4.3.5 Randomized double-layer hole array

Finally, we return to one of the perforated double-layer structures (Section 4.3.1), but with a twist: *randomly* distributed holes in gold-VO_2 (Figure 4.17), with the same nominal hole diameter and areal hole coverage as in the periodic Au-VO_2 array (Figure 4.9). The purpose of measuring the transmission of a randomized hole array was to reinforce our claim that the reverse switching we observed in the case of periodic metal-VO_2 arrays was caused by reduction in the permittivity contrast *inside* the holes and not between the two interfaces of the noble-metal film. The effect of the latter was discussed earlier in connection with Figure 4.7, where matching the refractive indices of the input and output interfaces produced a stronger EOT effect. On the other hand, a randomized hole array cannot sustain coherent surface modes due to the lack of periodicity, and hence no extraordinary transmission is expected as the EOT effect relies on in-phase multi-scattering and interference processes between neighboring rows in a periodic hole array.[144] Indeed, the transmission spectra of our randomized Au-VO_2 holes (Figure 4.18) differ qualitatively from the EOT spectra of the periodic array in the same double-layer film (Figure 4.11b). Instead of a sequence of relatively sharp dips and peaks, the random-holes spectra exhibit

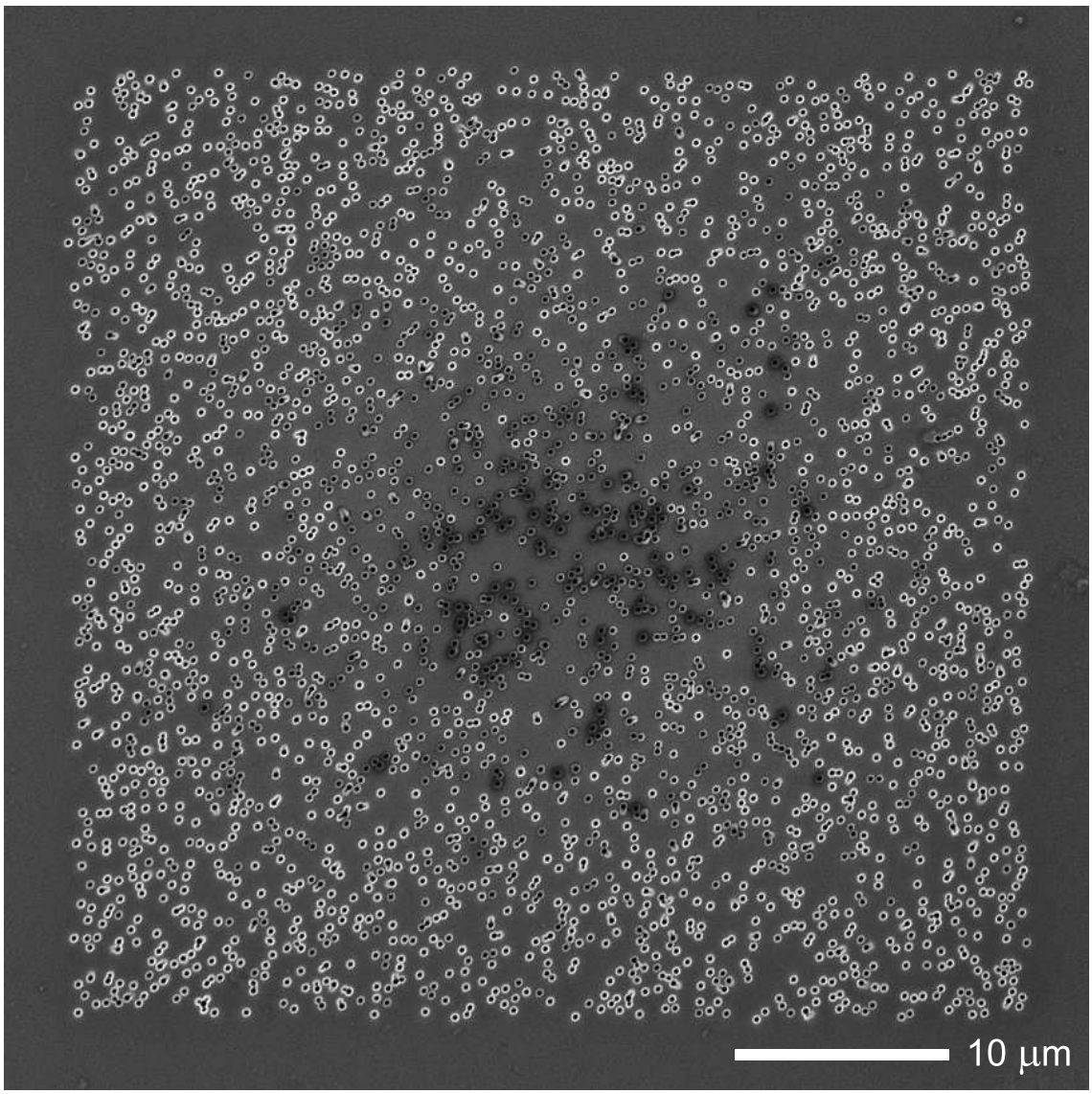

Figure 4.17: FIB micrograph of randomized array of 3600 circular holes in Au-VO_2 double layer on glass. *Parameters*: $d = 250$ nm, $t_{Au} = 230$ nm, $t_{VO_2} = 200$ nm.

a rather broad peak reminiscent of the transmission of an isolated hole in a metal film, which can be attributed to the excitation of a localized surface-plasmon resonance (LSPR) at the aperture ridge.[175,186] The crucial finding here is that the random-holes transmission is also reversed—the holes transmit more in the metallic phase of the VO_2 layer (Figure 4.18), independently of the EOT phenomenon. To recapitulate, our model attributes this reversal to the *reduction of losses* from diffuse scattering and leaky waves for metallic-phase

VO_2 at near-IR wavelengths, by virtue of the lower permittivity contrast between air and VO_2 (Figure 4.19).

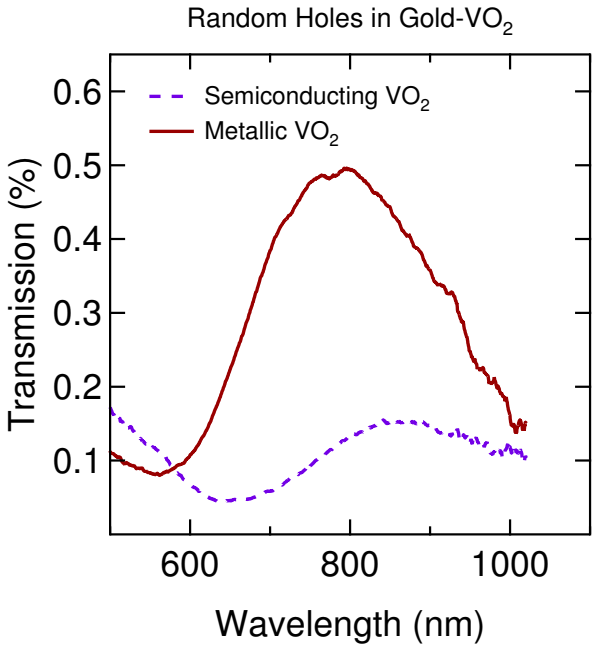

Figure 4.18: Experimental zero-order, normal-incidence transmission spectra, in each VO_2 phase, for randomized hole array in Au-VO_2 double layer. Note that the random holes also exhibit the *reverse switching* effect.

4.3.6 Prospects for all-optical modulation of EOT

Since the electronic response of the plasmonic material in these structures is fast on the femtosecond timescale, it is logical to ask whether the EOT effect can likewise be modulated on an ultrafast timescale. Experiments by Cavalleri *et al.* on VO_2 films show that hole doping effected by a femtosecond laser pulse can initiate the semiconductor-to-metal transition (SMT) within a few hundred femtoseconds.[187] The details of the ultrafast response, however, are dependent on the thickness of the film. More recent X-ray studies seem to indicate that for 800-nm incident laser light, the turn-on response of the film is

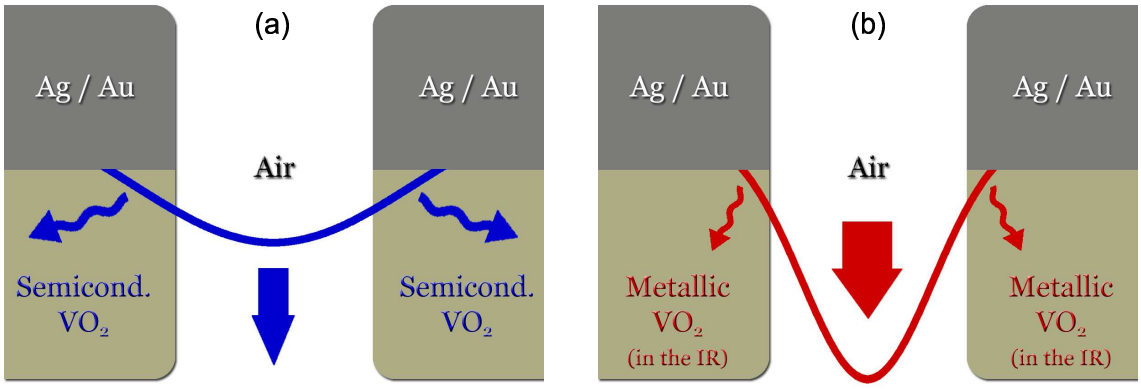

Figure 4.19: Schematics of transmission through hole in Ag/Au-VO_2 structure during the **(a)** semiconducting and **(b)** metallic phase of the VO_2 layer. The zero-order transmission is higher in the metallic-phase of the VO_2 layer because of the lower permittivity contrast between the hole interior ($\varepsilon_{\text{air}} = 1$) and the surrounding VO_2 (*e.g.*, $\varepsilon'\{met.\ VO_2\ @\ 980\ \text{nm}\} \approx 1$ *vs.* $\varepsilon'\{semi.\ VO_2\ @\ 980\ \text{nm}\} \approx 9$).

extremely fast for film thicknesses of 70 nm or less, but diffusive after that.[31] This ultrafast response depth is, of course, a function of the excitation wavelength, and it is possible that a laser wavelength with greater penetration depth in VO_2 could achieve ultrafast SMT initiation for thicker films. The response time also appears to be a function of fluence, with important dynamical features showing a differentiated response below the 100-fs timescale.[69]

The more challenging question for ultrafast modulation is whether or not the SMT can be turned off at a fast timescale. Evidence so far indicates that the return from the metallic to the semiconducting phase occurs on nanosecond or sub-nanosecond time scales, governed essentially by thermal diffusivity.[188,189] While the metallic state relaxes on a sub-picosecond timescale for near-threshold densities of photo-initiated electron-hole pairs, the relaxation times increase significantly with increasing electron-hole plasma density, even for rather thin VO_2 films on diamond substrates.[1] In the case of our double-layer plasmonic structures, it is nevertheless plausible that the thermal conductivity of the noble metal would assist the cooling transition back to the semiconducting state. Hence the question of possible ultrafast turn-on *and* turn-off of plasmonic effects remains open.

4.4 Summary

In generic terms, the future of optoelectronic devices relies on the ability to manipulate light on a subwavelength scale, where diffraction-limited optical components lose their utility. Here we have presented a novel way to control the *extraordinary optical transmission* through subwavelength hole arrays in structures composed of a VO_2 thin film sandwiched between an opaque metal layer and a transparent substrate. The control mechanism relies on the thermally induced metal-semiconductor transition of VO_2, but the transition can take place on a sub-picosecond timescale if triggered by a laser pulse, which opens the possibility for ultrafast switching devices. The present work has uncovered a counterintuitive trend in the near-IR transmission properties of the perforated VO_2 layer when compared to a continuous VO_2 film of the same thickness, which we call *reverse switching*. Under these conditions, the zero-order transmitted intensity from perforated Ag-VO_2 or Au-VO_2 double layers on glass is, in fact, considerably higher during the metallic phase of the VO_2 material than it is during the semiconducting phase. A simple heuristic model seems sufficient to account qualitatively for this effect, based on the idea that the losses in the zero-order transmission are caused by evanescent waves with varying leakage into the VO_2 layer, depending on the VO_2 state; in addition, diffuse scattering at the entrance and exit apertures also contributes. The magnitude of these losses increases with higher permittivity contrast between the interior and exterior of the holes. The role of metallic VO_2 in further enhancing the EOT from perforated silver or gold films has been emphasized by comparing measurements on perforated and non-perforated areas of the same VO_2 film, which showed that the zero-order high-temperature transmission through a VO_2 hole array can exceed the direct transmission through the flat film. A major point in the qualitative model is that the holey films with nanoscale dimensions, with or without the metal, constitute a very large effective interfacial area for the incident photons. The observed effects are thus directly related to the ability to construct such nanoscale structures.

REFERENCES

[1] C. Kübler, H. Ehrke, R. Huber, R. Lopez, A. Halabica, R. F. Haglund, and A. Leitenstorfer, *Physical Review Letters* **99**, 116401 (2007).

[2] M. M. Qazilbash, M. Brehm, B. G. Chae, P. C. Ho, G. O. Andreev, B. J. Kim, S. J. Yun, A. V. Balatsky, M. B. Maple, F. Keilmann, H. T. Kim, and D. N. Basov, *Science* **318**, 1750 (2007).

[3] P. Baum, D. S. Yang, and A. H. Zewail, *Science* **318**, 788 (2007).

[4] A. Sharoni, J. G. Ramírez, and I. K. Schuller, *Physical Review Letters* **101**, 026404 (2008).

[5] R. Lopez, T. E. Haynes, L. A. Boatner, L. C. Feldman, and R. F. Haglund, *Physical Review B* **65**, 224113 (2002).

[6] T. W. Ebbesen, H. J. Lezec, H. F. Ghaemi, T. Thio, and P. A. Wolff, *Nature* **391**, 667 (1998).

[7] T. J. Kim, T. Thio, T. W. Ebbesen, D. E. Grupp, and H. J. Lezec, *Optics Letters* **24**, 256 (1999).

[8] J. Dintinger, A. Degiron, and T. W. Ebbesen, *MRS Bulletin* **30**, 381 (2005).

[9] R. Lopez, L. C. Feldman, and R. F. Haglund, *Physical Review Letters* **93**, 177403 (2004).

[10] C. X. Wang and G. W. Yang, *Materials Science & Engineering R: Reports* **49**, 157 (2005).

[11] J. G. Lee and H. Mori, *Physical Review Letters* **93**, 235501 (2004).

[12] K. K. Nanda, A. Maisels, F. E. Kruis, H. Fissan, and S. Stappert, *Physical Review Letters* **91**, 106102 (2003).

[13] T. Shibata, B. A. Bunker, Z. Y. Zhang, D. Meisel, C. F. Vardeman, and J. D. Gezelter, *Journal of the American Chemical Society* **124**, 11989 (2002).

[14] T. Shinohara, T. Sato, and T. Taniyama, *Physical Review Letters* **91**, 197201 (2003).

[15] H. J. Mamin, R. Budakian, B. W. Chui, and D. Rugar, *Physical Review Letters* **91**, 207604 (2003).

[16] K. Dick, T. Dhanasekaran, Z. Zhang, and D. Meisel, *Journal of the American Chemical Society* **124**, 2312 (2002).

[17] R. A. Masumura, P. M. Hazzledine, and C. S. Pande, *Acta Materialia* **46**, 4527 (1998).

[18] D. Katz, T. Wizansky, O. Millo, E. Rothenberg, T. Mokari, and U. Banin, *Physical Review Letters* **89**, 199901 (2002).

[19] J. T. Lau, A. Fohlisch, R. Nietubyc, M. Reif, and W. Wurth, *Physical Review Letters* **89**, 057201 (2002).

[20] C. Voisin, D. Christofilos, N. D. Fatti, F. Vallee, B. Prevel, E. Cottancin, J. Lerme, M. Pellarin, and M. Broyer, *Physical Review Letters* **85**, 2200 (2000).

[21] F. J. Morin, *Physical Review Letters* **3**, 34 (1959).

[22] J. B. Goodenough, *Journal of Solid State Chemistry* **3**, 490 (1971).

[23] M. Imada, A. Fujimori, and Y. Tokura, *Reviews of Modern Physics* **70**, 1039 (1998).

[24] P. A. Cox, *Transition metal oxides: An introduction to their electronic structure and properties*, The International Series of Monographs on Chemistry, Clarendon Press; Oxford University Press, Oxford New York, 1992.

[25] A. Zylbersztejn and N. F. Mott, *Physical Review B* **11**, 4383 (1975).

[26] D. Paquet and P. L. Hugon, *Physical Review B* **22**, 5284 (1980).

[27] R. M. Wentzcovitch, W. W. Schulz, and P. B. Allen, *Physical Review Letters* **73**, 3043 (1994).

[28] T. M. Rice, H. Launois, and J. P. Pouget, *Physical Review Letters* **73**, 3042 (1994).

[29] R. M. Wentzcovitch, W. W. Schulz, and P. B. Allen, *Physical Review Letters* **72**, 3389 (1994).

[30] S. Biermann, A. Poteryaev, A. I. Lichtenstein, and A. Georges, *Physical Review Letters* **94**, 026404 (2005).

[31] A. Cavalleri, T. Dekorsy, H. H. W. Chong, J. C. Kieffer, and R. W. Schoenlein, *Physical Review B* **70**, 161102 (2004).

[32] H. T. Kim, Y. W. Lee, B. J. Kim, B. G. Chae, S. J. Yun, K. Y. Kang, K. J. Han, K. J. Yee, and Y. S. Lim, *Physical Review Letters* **97**, 266401 (2006).

[33] A. Cavalleri, M. Rini, and R. W. Schoenlein, *Journal of the Physical Society of Japan* **75**, 011004 (2006).

[34] V. S. Vikhnin, S. Lysenko, A. Rua, F. Fernandez, and H. Liu, *Solid State Communications* **137**, 615 (2006).

[35] S. Lysenko, A. J. Rua, V. Vikhnin, J. Jimenez, F. Fernandez, and H. Liu, *Applied Surface Science* **252**, 5512 (2006).

[36] M. S. Grinolds, V. A. Lobastov, J. Weissenrieder, and A. H. Zewail, *Proceedings of the National Academy of Sciences of the United States of America* **103**, 18427 (2006).

[37] I. Yamashita, H. Kawaji, T. Atake, Y. Kuroiwa, and A. Sawada, *Physical Review B* **68**, 092104 (2003).

[38] A. S. Shirinyan and M. Wautelet, *Nanotechnology* **15**, 1720 (2004).

[39] G. F. Goya, M. Veith, R. Rapalavicuite, H. Shen, and S. Mathur, *Applied Physics A: Materials Science & Processing* **80**, 1523 (2005).

[40] K. Jacobs, J. Wickham, and A. P. Alivisatos, *Journal of Physical Chemistry B* **106**, 3759 (2002).

[41] D. Zaziski, S. Prilliman, E. C. Scher, M. Casula, J. Wickham, S. M. Clark, and A. P. Alivisatos, *Nano Letters* **4**, 943 (2004).

[42] Q. Xu, I. D. Sharp, C. W. Yuan, D. O. Yi, C. Y. Liao, A. M. Glaeser, A. M. Minor, J. W. Beeman, M. C. Ridgway, P. Kluth, I. Ager, J. W., D. C. Chrzan, and E. E. Haller, *Physical Review Letters* **97**, 155701 (2006).

[43] R. E. Cech and D. Turnbull, *Journal of Metals* , 124 (1956).

[44] I. W. Chen, Y. H. Chiao, and K. Tsuzaki, *Acta Metallurgica* **33**, 1847 (1985).

[45] J. Y. Suh, R. Lopez, L. C. Feldman, and R. F. Haglund, *Journal of Applied Physics* **96**, 1209 (2004).

[46] D. Brassard, S. Fourmaux, M. Jean-Jacques, J. C. Kieffer, and M. A. El Khakani, *Applied Physics Letters* **87**, 051910 (2005).

[47] R. A. Aliev, V. N. Andreev, V. M. Kapralova, V. A. Klimov, A. I. Sobolev, and E. B. Shadrin, *Physics of the Solid State* **48**, 929 (2006).

[48] J. Rozen, R. Lopez, R. F. Haglund, and L. C. Feldman, *Applied Physics Letters* **88**, 081902 (2006).

[49] K. Nagashima, T. Yanagida, H. Tanaka, and T. Kawai, *Journal of Applied Physics* **101**, 026103 (2007).

[50] R. Lopez, L. A. Boatner, T. E. Haynes, R. F. Haglund, and L. C. Feldman, *Applied Physics Letters* **79**, 3161 (2001).

[51] R. Lopez, L. A. Boatner, T. E. Haynes, L. C. Feldman, and R. F. Haglund, *Journal of Applied Physics* **92**, 4031 (2002).

[52] R. Lopez, T. E. Haynes, L. A. Boatner, L. C. Feldman, and R. F. Haglund, *Optics Letters* **27**, 1327 (2002).

[53] R. Lopez, J. Y. Suh, L. C. Feldman, and R. F. Haglund, *Symposium Proceedings of the Materials Research Society* **820**, R1.5 (2004).

[54] M. Rini, A. Cavalleri, R. W. Schoenlein, R. Lopez, L. C. Feldman, R. F. Haglund, L. A. Boatner, and T. E. Haynes, *Optics Letters* **30**, 558 (2005).

[55] V. Eyert, *Annalen der Physik* **11**, 650 (2002).

[56] M. M. Qazilbash, K. S. Burch, D. Whisler, D. Shrekenhamer, B. G. Chae, H. T. Kim, and D. N. Basov, *Physical Review B* **74**, 205118 (2006).

[57] H. W. Verleur, A. S. Barker, and C. N. Berglund, *Physical Review* **172**, 788 (1968).

[58] S. Shin, S. Suga, M. Taniguchi, M. Fujisawa, H. Kanzaki, A. Fujimori, H. Daimon, Y. Ueda, K. Kosuge, and S. Kachi, *Physical Review B* **41**, 4993 (1990).

[59] M. M. Qazilbash, A. A. Schafgans, K. S. Burch, S. J. Yun, B. G. Chae, B. J. Kim, H. T. Kim, and D. N. Basov, *Physical Review B* **77**, 115121 (2008).

[60] S. Lysenko, V. Vikhnin, F. Fernandez, A. Rua, and H. Liu, *Physical Review B* **75**, 075109 (2007).

[61] C. Kittel, *Introduction to solid state physics*, Wiley, New York, 7th edition, 1996.

[62] J. Spalek, Superconductivity mechanisms, in *Encyclopedia of Modern Physics*, edited by R. A. Meyers and S. N. Shore, pp. 679–716, Academic Press, San Diego, 1990.

[63] T. M. Rice and D. B. McWhan, *IBM Journal of Research and Development* **14**, 251 (1970).

[64] N. F. Mott, *Reviews of Modern Physics* **40**, 677 (1968).

[65] J. Hubbard, *Proceedings of the Royal Society of London. Series A, Mathematical and Physical Sciences* **276**, 238 (1963).

[66] A. I. Buzdin and L. N. Bulayevskii, *Uspekhi Fizicheskikh Nauk* **131**, 495 (1980).

[67] J. M. Tomczak and S. Biermann, *Journal of Physics: Condensed Matter* **19**, 365206 (2007).

[68] M. W. Haverkort, Z. Hu, A. Tanaka, W. Reichelt, S. V. Streltsov, M. A. Korotin, V. I. Anisimov, H. H. Hsieh, H. J. Lin, C. T. Chen, D. I. Khomskii, and L. H. Tjeng, *Physical Review Letters* **95**, 196404 (2005).

[69] C. Kübler, H. Ehrke, A. Leitenstorfer, R. Lopez, A. Halabica, and R. F. Haglund, Ultrafast Conductivity and Lattice Dynamics of Insulator-Metal Phase Transition in VO2 Studied via Multi-Terahertz Spectroscopy, in *Joint 31st Int'l Conference on Infrared and Millimeter Waves and 14th Int'l Conference on Terahertz Electronics (IRMMW-THz'06)*, Shanghai, China, 2006.

[70] C. N. R. Rao and K. J. Rao, *Phase transitions in solids: an approach to the study of the chemistry and physics of solids*, McGraw-Hill, New York, 1978.

[71] C. N. Berglund and H. J. Guggenheim, *Physical Review* **185**, 1022 (1969).

[72] J. Ortín, A. Planes, and L. Delaey, Hysteresis in Shape-Memory Materials, in *The Science of Hysteresis*, edited by G. Bertotti and I. D. Mayergoyz, volume 3, pp. 467–553, Elsevier, London, 2005.

[73] L. Delaey, Diffusionless Transformations, in *Phase Transformations in Materials*, edited by G. Kostorz, pp. 583–654, Wiley-VCH, Weinheim; New York; Chichester, new edition, 2001.

[74] P. C. Clapp, *Journal de Physique IV* **5**, 11 (1995).

[75] I. A. Khakhaev, F. A. Chudnovskii, and E. B. Shadrin, *Fizika Tverdogo Tela* **36**, 1643 (1994).

[76] H. S. Choi, J. S. Ahn, J. H. Jung, T. W. Noh, and D. H. Kim, *Physical Review B* **54**, 4621 (1996).

[77] F. J. Perez-Reche, E. Vives, L. Manosa, and A. Planes, *Physical Review Letters* **8719**, 195701 (2001).

[78] D. Maurer, A. Leue, R. Heichele, and V. Müller, *Physical Review B* **60**, 13249 (1999).

[79] J. Narayan and V. M. Bhosle, *Journal of Applied Physics* **100**, 103524 (2006).

[80] L. A. L. de Almeida, G. S. Deep, A. M. N. Lima, H. F. Neff, and R. C. S. Freire, *Ieee Transactions on Instrumentation and Measurement* **50**, 1030 (2001).

[81] V. A. Klimov, I. O. Timofeeva, S. D. Khanin, E. B. Shadrin, A. V. Ilinskii, and F. Silva-Andrade, *Technical Physics* **47**, 1134 (2002).

[82] R. A. Aliev and V. A. Klimov, *Physics of the Solid State* **46**, 532 (2004).

[83] R. A. Aliev, V. N. Andreev, V. A. Klimov, V. M. Lebedev, S. E. Nikitin, E. I. Terukov, and E. B. Shadrin, *Technical Physics* **50**, 754 (2005).

[84] W. Haidinger and D. Gross, *Thin Solid Films* **12**, 433 (1972).

[85] Y. Muraoka and Z. Hiroi, *Applied Physics Letters* **80**, 583 (2002).

[86] G. Xu, P. Jin, M. Tazawa, and K. Yoshimura, *Applied Surface Science* **244**, 449 (2005).

[87] E. Kusano and J. A. Theil, *Journal of Vacuum Science & Technology A: Vacuum Surfaces and Films* **7**, 1314 (1989).

[88] V. A. Klimov, I. O. Timofeeva, S. D. Khanin, E. B. Shadrin, A. V. Il'inskii, and F. Silva-Andrade, *Semiconductors* **37**, 370 (2003).

[89] F. Beteille and J. Livage, *Journal of Sol-Gel Science and Technology* **13**, 915 (1998).

[90] W. Burkhardt, T. Christmann, B. K. Meyer, W. Niessner, D. Schalch, and A. Scharmann, *Thin Solid Films* **345**, 229 (1999).

[91] E. Cavanna, J. P. Segaud, and J. Livage, *Materials Research Bulletin* **34**, 167 (1999).

[92] F. C. Case, *Journal of Vacuum Science & Technology A: Vacuum Surfaces and Films* **2**, 1509 (1984).

[93] F. C. Case, *Journal of Vacuum Science & Technology A: Vacuum Surfaces and Films* **7**, 1194 (1989).

[94] A. Leone, A. M. Trione, and F. Junga, *IEEE Transactions on Nuclear Science* **37**, 1739 (1990).

[95] P. Jin, S. Nakao, and S. Tanemura, *Nuclear Instruments & Methods in Physics B: Beam Interactions with Materials & Atoms* **141**, 419 (1998).

[96] L. B. Lin, T. C. Lu, Q. Liu, Y. Lu, and X. D. Feng, *Surface & Coatings Technology* **158**, 530 (2002).

[97] F. Beteille, L. Mazerolles, and J. Livage, *Materials Research Bulletin* **34**, 2177 (1999).

[98] C. Petit, J. M. Frigerio, and M. Goldmann, *Journal of Physics-Condensed Matter* **11**, 3259 (1999).

[99] K. Y. Tsai, T. S. Chin, H. P. D. Shieh, and C. H. Ma, *Journal of Materials Research* **19**, 2306 (2004).

[100] I. Karakurt, J. Boneberg, P. Leiderer, R. Lopez, A. Halabica, and R. F. Haglund, *Applied Physics Letters* **91**, 091907 (2007).

[101] J. E. Mahan, *Physical vapor deposition of thin films*, Wiley, New York; Chichester, 2000.

[102] O. Svelto, S. Longhi, G. D. Valle, S. Kück, G. Huber, M. Pollnau, and H. Hillmer etc., Lasers and Coherent Light Sources, in *Springer Handbook of Lasers and Optics*, edited by F. Träger, pp. 583–936, Springer, New York, 2007.

[103] N. D. Bassim, P. K. Schenck, E. U. Donev, E. J. Heilweil, E. Cockayne, M. L. Green, and L. C. Feldman, *Applied Surface Science* **254**, 785 (2007).

[104] C. A. Volkert and A. M. Minor, *MRS Bulletin* **32**, 389 (2007).

[105] P. Rai-Choudhury, *Handbook of Microlithography, Micromachining, and Microfabrication*, volume 1, SPIE Optical Engineering Press; Institution of Electrical Engineers, Bellingham, Wash., USA London, UK, 1997.

[106] T. L. Alford, L. C. Feldman, and J. W. Mayer, *Fundamentals of nanoscale film analysis*, Springer, New York; London, 2007.

[107] M. Mayer, *SIMNRA (ver. 5.02)*, http://www.ipp.mpg.de/∼mam, 2004.

[108] K. Iizuka, *Elements of photonics*, Wiley Series in Pure and Applied Optics, Wiley, New York, 2002.

[109] WITec, *AlphaSNOM Manual*, WITec Wissenschaftliche Instrumente und Technologie GmbH, 2002.

[110] M. Fox, *Optical properties of solids*, Oxford Master Series in Condensed Matter Physics, Oxford University Press, Oxford; New York, 2001.

[111] G. Brooker, *Modern classical optics*, Oxford University Press, Oxford, 2003.

[112] L. Novotny and B. Hecht, *Principles of Nano-Optics*, Cambridge University Press, 2006.

[113] S. A. Maier and H. A. Atwater, *Journal of Applied Physics* **98**, 011101 (2005).

[114] U. Kreibig, M. Gartz, A. Hilger, and H. Hovel, *Optical investigations of surfaces and interfaces of metal clusters*, volume 4, JAI Press, Inc., Stanford, 1998.

[115] K. L. Kelly, E. Coronado, L. L. Zhao, and G. C. Schatz, *Journal of Physical Chemistry B* **107**, 668 (2003).

[116] J. D. Jackson, *Classical electrodynamics*, Wiley, New York, 3rd edition, 1999.

[117] M. L. Sandrock and C. A. Foss, *Journal of Physical Chemistry B* **103**, 11398 (1999).

[118] G. Mie, *Annalen der Physik* **25**, 377 (1908).

[119] I. W. Sudiarta and P. Chylek, *Journal of the Optical Society of America A* **18**, 1275 (2001).

[120] H. C. van de Hulst, *Light Scattering by Small Particles*, Dover Publications, Inc., New York, 1981.

[121] M. B. Cortie, A. Dowd, N. Harris, and M. J. Ford, *Physical Review B* **75**, 113405 (2007).

[122] L. R. Hirsch, R. J. Stafford, J. A. Bankson, S. R. Sershen, B. Rivera, R. E. Price, J. D. Hazle, N. J. Halas, and J. L. West, *Proceedings of the National Academy of Sciences of the United States of America* **100**, 13549 (2003).

[123] J. M. Brockman, B. P. Nelson, and R. M. Corn, *Annual Review of Physical Chemistry* **51**, 41 (2000).

[124] E. U. Donev, J. Y. Suh, F. Villegas, R. Lopez, R. F. Haglund, and L. C. Feldman, *Physical Review B* **73**, 201401 (2006).

[125] J. Y. Suh, E. U. Donev, R. Lopez, L. C. Feldman, and R. F. Haglund, *Applied Physics Letters* **88**, 133115 (2006).

[126] A. Bianconi, S. Stizza, and R. Bernardini, *Physical Review B* **24**, 4406 (1981).

[127] Y. N. Xia and N. J. Halas, *MRS Bulletin* **30**, 338 (2005).

[128] G. Xu, Y. Chen, M. Tazawa, and P. Jin, *Journal of Physical Chemistry B* **110**, 2051 (2006).

[129] E. A. Coronado and G. C. Schatz, *Journal of Chemical Physics* **119**, 3926 (2003).

[130] M. Maaza, O. Nemraoui, C. Sella, A. C. Beye, and B. Baruch-Barak, *Optics Communications* **254**, 188 (2005).

[131] W. Rechberger, A. Hohenau, A. Leitner, J. R. Krenn, B. Lamprecht, and F. R. Aussenegg, *Optics Communications* **220**, 137 (2003).

[132] J. Y. Suh, E. U. Donev, D. W. Ferrara, K. A. Tetz, L. C. Feldman, and R. F. Haglund, *Journal of Optics A: Pure and Applied Optics* , 055202 (2008).

[133] M. D. McMahon, R. Lopez, R. F. Haglund, E. A. Ray, and P. H. Bunton, *Physical Review B* **73**, 041401 (2006).

[134] S. Wang, D. F. P. Pile, C. Sun, and X. Zhang, *Nano Letters* **7**, 1076 (2007).

[135] C. A. Foss, G. L. Hornyak, J. A. Stockert, and C. R. Martin, *Journal of Physical Chemistry* **98**, 2963 (1994).

[136] J. Grand, P. M. Adam, A. S. Grimault, A. Vial, M. L. De la Chapelle, J. L. Bijeon, S. Kostcheev, and P. Royer, *Plasmonics* **1**, 135 (2006).

[137] K. H. Su, Q. H. Wei, X. Zhang, J. J. Mock, D. R. Smith, and S. Schultz, *Nano Letters* **3**, 1087 (2003).

[138] T. R. Jensen, M. L. Duval, K. L. Kelly, A. A. Lazarides, G. C. Schatz, and R. P. Van Duyne, *Journal of Physical Chemistry B* **103**, 9846 (1999).

[139] J. J. Mock, D. R. Smith, and S. Schultz, *Nano Letters* **3**, 485 (2003).

[140] P. B. Johnson and R. W. Christy, *Physical Review B* **6**, 4370 (1972).

[141] S. Link and M. A. El-Sayed, *Journal of Physical Chemistry B* **103**, 4212 (1999).

[142] H. Bethe, *Physical Review* **66**, 163 (1944).

[143] C. J. Bouwkamp, *IEEE Transactions on Antennas and Propagation* **AP18**, 152 (1970).

[144] H. Liu and P. Lalanne, *Nature* **452**, 728 (2008).

[145] C. Liu, V. Kamaev, and Z. V. Vardeny, *Applied Physics Letters* **86**, 143501 (2005).

[146] A. Krishnan, T. Thio, T. J. Kima, H. J. Lezec, T. W. Ebbesen, P. A. Wolff, J. Pendry, L. Martin-Moreno, and F. J. Garcia-Vidal, *Optics Communications* **200**, 1 (2001).

[147] E. Hendry, M. J. Lockyear, J. Gómez-Rivas, L. Kuipers, and M. Bonn, *Physical Review B* **75**, 235305 (2007).

[148] E. U. Donev, J. Y. Suh, R. Lopez, L. C. Feldman, and R. F. Haglund, *Advances in OptoElectronics* , 739135 (2008).

[149] S. G. Tikhodeev, A. L. Yablonskii, E. A. Muljarov, N. A. Gippius, and T. Ishihara, *Physical Review B* **66**, 045102 (2002).

[150] A. Roberts, *Journal of the Optical Society of America A: Optics Image Science and Vision* **4**, 1970 (1987).

[151] A. Liebsch, *Physical Review Letters* **71**, 145 (1993).

[152] W. L. Barnes, *Journal of Optics A: Pure and Applied Optics* **8**, S87 (2006).

[153] H. Raether, *Springer Tracts in Modern Physics* **111**, 1 (1988).

[154] W. L. Barnes, A. Dereux, and T. W. Ebbesen, *Nature* **424**, 824 (2003).

[155] A. V. Zayats, L. Salomon, and F. de Fornel, *Journal of Microscopy* **210**, 344 (2003).

[156] H. F. Ghaemi, T. Thio, D. E. Grupp, T. W. Ebbesen, and H. J. Lezec, *Physical Review B* **58**, 6779 (1998).

[157] D. S. Kim, S. C. Hohng, V. Malyarchuk, Y. C. Yoon, Y. H. Ahn, K. J. Yee, J. W. Park, J. Kim, Q. H. Park, and C. Lienau, *Physical Review Letters* **91**, 143901 (2003).

[158] P. Lalanne, J. C. Rodier, and J. P. Hugonin, *Journal of Optics A: Pure and Applied Optics* **7**, 422 (2005).

[159] E. Popov, M. Neviere, S. Enoch, and R. Reinisch, *Physical Review B* **62**, 16100 (2000).

[160] S. Enoch, E. Popov, M. Neviere, and R. Reinisch, *Journal of Optics A: Pure and Applied Optics* **4**, S83 (2002).

[161] T. Thio, H. F. Ghaemi, H. J. Lezec, P. A. Wolff, and T. W. Ebbesen, *Journal of the Optical Society of America B: Optical Physics* **16**, 1743 (1999).

[162] L. Martin-Moreno, F. J. Garcia-Vidal, H. J. Lezec, K. M. Pellerin, T. Thio, J. B. Pendry, and T. W. Ebbesen, *Physical Review Letters* **86**, 1114 (2001).

[163] S. A. Darmanyan and A. V. Zayats, *Physical Review B* **67**, 035424 (2003).

[164] W. L. Barnes, W. A. Murray, J. Dintinger, E. Devaux, and T. W. Ebbesen, *Physical Review Letters* **92**, 107401 (2004).

[165] H. J. Lezec and T. Thio, *Optics Express* **12**, 3629 (2004).

[166] G. Gay, O. Alloschery, B. V. De Lesegno, C. O'Dwyer, J. Weiner, and H. J. Lezec, *Nature Physics* **2**, 262 (2006).

[167] G. Gay, O. Alloschery, B. V. de Lesegno, J. Weiner, and H. J. Lezec, *Physical Review Letters* **96**, 213901 (2006).

[168] G. Gay, O. Alloschery, J. Weiner, H. J. Lezec, C. O'Dwyer, M. Sukharev, and T. Seideman, *Physical Review E* **75**, 016612 (2007).

[169] P. Lalanne and J. P. Hugonin, *Nature Physics* **2**, 551 (2006).

[170] F. Kalkum, G. Gay, O. Alloschery, J. Weiner, H. J. Lezec, Y. Xie, and M. Mansuripur, *Optics Express* **15**, 2613 (2007).

[171] G. Gay, O. Alloschery, J. Weiner, H. J. Lezec, C. O'Dwyer, M. Sukharev, and T. Seideman, *Nature Physics* **2**, 792 (2006).

[172] F. J. Garcia-Vidal, S. G. Rodrigo, and L. Martin-Moreno, *Nature Physics* **2**, 790 (2006).

[173] P. Lalanne, J. P. Hugonin, M. Besbes, and P. Bienstman, *Nature Physics* **2**, 792 (2006).

[174] J. Weiner and H. J. Lezec, *Nature Physics* **2**, 791 (2006).

[175] A. Degiron and T. W. Ebbesen, *Journal of Optics A: Pure and Applied Optics* **7**, S90 (2005).

[176] C. Genet, M. P. van Exter, and J. P. Woerdman, *Optics Communications* **225**, 331 (2003).

[177] M. Sarrazin and J. P. Vigneron, *Physical Review E* **68**, 016603 (2003).

[178] M. Sarrazin, J. P. Vigneron, and J. M. Vigoureux, *Physical Review B* **67**, 085415 (2003).

[179] A. Degiron, H. J. Lezec, W. L. Barnes, and T. W. Ebbesen, *Applied Physics Letters* **81**, 4327 (2002).

[180] K. L. van der Molen, F. B. Segerink, N. F. van Hulst, and L. Kuipers, *Applied Physics Letters* **85**, 4316 (2004).

[181] A. Hessel and A. A. Oliner, *Applied Optics* **4**, 1275 (1965).

[182] F. J. Garcia de Abajo, *Reviews of Modern Physics* **79**, 1267 (2007).

[183] J. E. Stewart and W. S. Gallaway, *Applied Optics* **1**, 421 (1962).

[184] E. D. Palik, *Handbook of optical constants of solids*, Academic Press Handbook Series, Academic Press, Orlando, 1985.

[185] W. Bogaerts, P. Bienstman, D. Taillaert, R. Baets, and D. De Zutter, *IEEE Photonics Technology Letters* **13**, 565 (2001).

[186] A. Degiron, H. J. Lezec, N. Yamamoto, and T. W. Ebbesen, *Optics Communications* **239**, 61 (2004).

[187] A. Cavalleri, C. Tóth, C. W. Siders, J. A. Squier, F. Ráksi, P. Forget, and J. C. Kieffer, *Physical Review Letters* **87**, 237401 (2001).

[188] M. F. Becker, A. B. Buckman, R. M. Walser, T. Lepine, P. Georges, and A. Brun, *Applied Physics Letters* **65**, 1507 (1994).

[189] M. F. Becker, A. B. Buckman, R. M. Walser, T. Lepine, P. Georges, and A. Brun, *Journal of Applied Physics* **79**, 2404 (1996).

[190] K. C. Kam and A. K. Cheetham, *Materials Research Bulletin* **41**, 1015 (2006).

[191] J. Park, I. H. Oh, E. Lee, K. W. Lee, C. E. Lee, K. Song, and Y. J. Kim, *Applied Physics Letters* **91**, 153112 (2007).

[192] F. Guinneton, L. Sauques, J. C. Valmalette, F. Cros, and J. R. Gavarri, *Journal of Physics and Chemistry of Solids* **62**, 1229 (2001).

[193] S. Q. Xu, H. P. Ma, S. X. Dai, and Z. H. Jiang, *Journal of Materials Science* **39**, 489 (2004).

[194] S. A. Pauli, R. Herger, P. R. Willmott, E. U. Donev, J. Y. Suh, and R. F. Haglund, *Journal of Applied Physics* **102**, 073527 (2007).

[195] K. Hyun-Tak, C. Byung-Gyu, Y. Doo-Hyeb, K. Gyungock, K. Kwang-Yong, L. Seung-Joon, K. Kwan, and L. Yong-Sik, *Applied Physics Letters* **86**, 242101 (2005).

[196] R. Srivastava and L. L. Chase, *Physical Review Letters* **27**, 727 (1971).

[197] M. Pan, J. Liu, H. M. Zhong, S. W. Wang, Z. F. Li, X. H. Chen, and W. Lu, *Journal of Crystal Growth* **268**, 178 (2004).

[198] G. I. Petrov, V. V. Yakovlev, and J. Squier, *Applied Physics Letters* **81**, 1023 (2002).

[199] J. C. Parker, *Physical Review B* **42**, 3164 (1990).

[200] H.-T. Yuan, K.-C. Feng, X.-J. Wang, C. Li, C.-J. He, and Y.-X. Nie, *Chinese Physics* , 82 (2004).

[201] P. Schilbe, *Physica B: Condensed Matter* **316**, 600 (2002).

[202] N. N. Brandt, O. O. Brovko, A. Y. Chikishev, and O. D. Paraschuk, *Applied Spectroscopy* **60**, 288 (2006).

[203] C. H. Griffiths and H. K. Eastwood, *Journal of Applied Physics* **45**, 2201 (1974).

[204] C. L. Xu, X. Ma, X. Liu, W. Y. Qiu, and Z. X. Su, *Materials Research Bulletin* **39**, 881 (2004).

[205] D. Dragoman and M. Dragoman, *Optical characterization of solids*, Springer, Berlin; New York, 2002.

[206] R. R. Andronenko, I. N. Goncharuk, V. Y. Davydov, F. A. Chudnovskii, and E. B. Shadrin, *Physics of the Solid State* **36**, 1136 (1994).

[207] P. Schilbe and D. Maurer, *Materials Science and Engineering A: Structural Materials Properties Microstructure and Processing* **370**, 449 (2004).

[208] H. H. Richardson, Z. N. Hickman, A. O. Govorov, A. C. Thomas, W. Zhang, and M. E. Kordesch, *Nano Letters* **6**, 783 (2006).

[209] A. O. Govorov, W. Zhang, T. Skeini, H. Richardson, J. Lee, and N. A. Kotov, *Nanoscale Research Letters* **1**, 84 (2006).

[210] G. A. Thomas, D. H. Rapkine, S. A. Carter, A. J. Millis, T. F. Rosenbaum, P. Metcalf, and J. M. Honig, *Physical Review Letters* **73**, 1529 (1994).

[211] S. Yonezawa, Y. Muraoka, Y. Ueda, and Z. Hiroi, *Solid State Communications* **129**, 245 (2004).

[212] F. C. Case, *Journal of Vacuum Science & Technology A: Vacuum Surfaces and Films* **9**, 461 (1991).

[213] H. Schuler, S. Grigoriev, and S. Horn, *Materials Research Society Symposium Proceedings* **474**, 291 (1997).

[214] B. Sass, C. Tusche, W. Felsch, N. Quaas, A. Weismann, and M. Wenderoth, *Journal of Physics: Condensed Matter* **16**, 77 (2004).

[215] P. A. Metcalf, S. Guha, L. P. Gonzalez, J. O. Barnes, E. B. Slamovich, and J. M. Honig, *Thin Solid Films* **515**, 3421 (2007).

[216] D. B. McWhan and J. P. Remeika, *Physical Review B* **2**, 3734 (1970).

[217] D. B. McWhan, A. Jayaraman, J. P. Remeika, and T. M. Rice, *Physical Review Letters* **34**, 547 (1975).

[218] P. Pfalzer, G. Obermeier, M. Klemm, S. Horn, and M. L. denBoer, *Physical Review B* **73**, 144106 (2006).

[219] S. Guimond, M. Abu Haija, S. Kaya, J. Lu, J. Weissenrieder, S. Shaikhutdinov, H. Kuhlenbeck, H. J. Freund, J. Dobler, and J. Sauer, *Topics in Catalysis* **38**, 117 (2006).

[220] Y. Jiang, S. Decker, C. Mohs, and K. J. Klabunde, *Journal of Catalysis* **180**, 24 (1998).

[221] N. Pinna, M. Antonietti, and M. Niederberger, *Colloids and Surfaces A: Physicochemical and Engineering Aspects* **250**, 211 (2004).

[222] C. V. Ramana, S. Utsunomiya, R. C. Ewing, and U. Becker, *Solid State Communications* **137**, 645 (2006).

[223] Z. H. Yang, P. J. Cai, L. Y. Chen, Y. L. Gu, L. Shi, A. W. Zhao, and Y. T. Qian, *Journal of Alloys and Compounds* **420**, 229 (2006).

[224] K. F. Zhang, J. S. Guo, C. H. Tao, X. Liu, H. L. Li, and Z. X. Su, *Chinese Journal of Inorganic Chemistry* **21**, 1090 (2005).

[225] K. F. Zhang, X. Z. Sun, G. W. Lou, X. Liu, H. L. Li, and Z. X. Su, *Materials Letters* **59**, 2729 (2005).